Aerospace Science and Technology, Volume 145, February 2024, Article number 108858
DOI:10.1016/j.ast.2023.108858

Adaptive multivariate reusable launch vehicles reentry attitude control with pre-specified performance in the presence of unmatched disturbances

Tianshuo Ge[1], Runqi Chai[1,2,*], Qinghua Zhu[1], Kaiyuan Chen[3,*], Antonios Tsourdos[2], Ishrak MD Farhan[1]

Abstract

This paper introduces a novel adaptive multivariable attitude control method for a reusable launch vehicle (RLV) to track desired attitude trajectories in the presence of unknown external disturbances and uncertainties. Unlike most existing designs that overlook mismatched disturbances, this method employs an adaptive finite-time observer (AFO) to estimate the unknown states. Based on the outputs of the AFO and the prescribed performance function, a time-varying adaptive gain that is not overestimated is designed to establish the adaptive multivariable attitude control for the RLV system. The simulations demonstrate that the proposed approach successfully guides the RLV to follow desired attitude signals despite the presence of unmatched disturbances and uncertainties.

Keywords: Finite time convergence, chattering attenuation, adaptive multivariable control, attitude control of reusable launch vehicle (RLV), pre-specified performance

1. Introduction

Reusable launch vehicles (RLVs) have become increasingly popular research subjects in the control community due to their high flight speed and wide range of applications in military and civilian domains [1–5]. However, RLVs possess unique characteristics, such as a lack of power during the reentry stage, a low lift-drag ratio, and significant changes in aerodynamic parameters. Moreover, RLVs are subjected to substantial external dynamic disturbances, such as altitude, wind, and payload variations. Therefore, designing an attitude controller for RLVs is a significant challenge that requires robustness to stabilize the model while considering the nonlinearities, uncertainties, and external disturbances [6].

*Corresponding author
Email addresses: 3120220827@bit.edu.cn (Tianshuo Ge), r.chai@bit.edu.cn, r.chai@cranfield.ac.uk (Runqi Chai), zqh1120190696@163.com (Qinghua Zhu), kaiyuanchen.mail.tsinghua.edu.cn (Kaiyuan Chen), a.tsourdos@cranfield.ac.uk (Antonios Tsourdos), i3498772052@126.com (Ishrak MD Farhan)
[1]School of Automation, Beijing Institute of Technology, Beijing, China
[2]School of Aerospace, Transport and Manufacturing, Cranfield University, UK
[3]Vanke School of Public Health, Tsinghua University, Beijing, China

Published by Elsevier. This is the Author Accepted Manuscript issued with: Creative Commons Attribution Non-Commercial No Derivatives License (CC:BY:NC:ND 4.0).
The final published version (version of record) is available online at DOI:10.1016/j.ast.2023.108858. Please refer to any applicable publisher terms of use.

Nonlinear control-based methods have gained widespread usage in controlling RLVs due to their ability to ensure stability and robustness. One such method is the planned gain approach, which is a standard technique utilized in RLV control to guarantee its stability and robustness [7]. However, maintaining a gain scheduling table with numerous gain values results in a significant computational burden and can impact the tracking performance along the nominal trajectory. To address this issue, alternative control methods, such as dynamic inversion [8] and feedback linearization [9], have been proposed to overcome the memory limitations.

Schierman proposed a nonlinear controller utilizing the dynamic inversion method to handle nonlinear problems [10]. However, accurately designing models for these controllers remains a challenging task. As such, several studies have explored various approaches to mitigate the impact of inaccurate models on the controller's performance. For instance, in [11], a backstepping control algorithm is proposed, which includes a finite-time command filter using auxiliary control signals and correction error compensation signals.The aforementioned issues are addressed by employing a centralized robust model predictive control (CRMPC) algorithm[12]. The authors have made advancements by developing a nonlinear feedback law, tightening system constraints, and incorporating a terminal controller with corresponding terminal region to achieve attitude tracking of Reusable Launch Vehicles subject to state/input constraints and uncertainties.

Sliding mode control (SMC) is another technique commonly employed to tackle uncertainties [13]. It is insensitive to matched disturbances and employs discontinuous injection to drive the sliding mode variables to zero within finite time [14]. The sliding mode technique is robust to external disturbances and mismatched equipment uncertainties, achieving the desired dynamic performance and significantly reducing preflight analysis time [15].

Shtessel et al. [16] proposed a multi-time-scale sliding mode controller that employs high-gain linear terms instead of discontinuous sign functions to reduce control jitter and achieve attitude tracking of RLV. Nevertheless, continuous control signals may compromise control accuracy and robustness. Talole and Patre [17] developed an SMC method driven by a perturbation observer to mitigate the control accuracy and robustness issues.

High-order sliding mode methods are often employed in RLV control due to their reduced control chattering phenomenon and improved tracking accuracy. A quasi-sliding mode controller based on higher-order sliding mode is proposed in [18].

These studies have successfully tackled the control instability issue arising from fuzzy models and demonstrated significant improvements in control performance compared to traditional methods. They exhibit exceptional robustness and the potential for efficient resource utilization.

However, the control methods discussed above assume limited and known disturbances. In practice, the aerodynamic characteristics of RLV are complex, and the upper limit of integrated disturbance is often unknown. To address

this issue, adaptive sliding mode control has been proposed. For instance, [19] presents an adaptive finite-time control algorithm based on hyper distortion for RLV systems with bounded perturbations and unknown upper bounds. Similarly, [20] proposes an adaptive distortion algorithm for RLV systems. The adaptive strategy employed in [19, 20] involves increasing the gain and then fixing it to ensure the finite-time convergence of the sliding variable when the sliding mode manifold is reached. These adaptive control approaches are crucial for enhancing the robustness and effectiveness of RLV control in the presence of complex and unknown disturbances.

The adaptive gains used in [19, 20] are overestimated, which can result in increased jitter caused by unmodeled dynamics [21]. To solve this problem, [22] proposes a new adaptive multivariable finite-time control algorithm for the UAV attitude control system. This method is based on the hyperwarping approach and employs the extended Kalman filter method.

The uncertainty in the RLV attitude system may not satisfy the matching conditions, which makes it challenging to develop sliding mode control (SMC) methods [23]. One of the main issues is that perturbations in the attitude angle system, such as unmodeled dynamics and aerodynamic coefficient perturbations, do not arise in the control channel. To address this issue, two types of approaches are currently designed. The first type uses disturbance observers (DO) to estimate mismatched disturbances, such as nonlinear DO [24] and finite-time DO [25]. SMC can then be used by redefining sliding mode variables that include uncertainty estimates [24, 26], or by combining backward inference techniques [27]. The controller based on a perturbation observer has been widely studied for unmatched attitude control systems and applied to RLV [26]. The second type redefines a new state variable with unknown uncertainties to turn the system into a matching structure [28]. State watchers have been used to estimate unknown states [29]. However, these approaches only achieve either exclusive stability or simplicity. For example, the research in [30] provides a relatively simple sliding mode control algorithm ensuring that the gain does not exceed the upper limit but cannot solve the problem of unmatched interference. In [20], the idea of a finite-time observer combined with adaptive twisting sliding mode control (ATSMC) was proposed. Although effective, it may not be convenient to apply in practice due to its complexity.

This paper proposes a new adaptive control algorithm that combines the Adaptive Finite-time Observer (AFO) and pre-specified performance Sliding Mode Control (PSMC) to solve the RLV attitude tracking problem. The proposed algorithm has non-overestimated adaptive gains and is easy to implement compared to related designs.

The contributions of this work are as follows:

1. This paper proposes a novel adaptive control algorithm that combines a simple control system with pre-specified performance sliding mode control (PSMC) to tackle the mismatch control problem in the RLV attitude system. The algorithm aims to enable the system to track the time-varying angle signal using the proposed control

scheme.

2. A finite time observer is utilized to group the mismatched interference into the angular rate. Moreover, a new state is defined to address the mismatched control problem in the RLV attitude system. Simulation results confirm the effectiveness of the proposed method in solving the problem at hand.
3. A pre-specified performance sliding mode control (PSMC) algorithm is developed using the selected finite time observer. The proposed algorithm is easy to implement, has fewer parameters, provides good control effects, and converges to the proposed control scheme's time. Moreover, the control designed in this paper ensures transient performance and robustness to external interference by preventing overestimation of the adaptive gain.

To the best of the author's knowledge, this paper presents for the first time the AFO-based PSMC scheme to ensure the feasibility and stability of the attitude tracking control problem for rigid RLV. The structure of this paper is organized as follows: Sec 2 defines the notation, the attitude dynamics model of RLV, and the control problem's objective. Sec 3 explains the design of the finite time observer required for this study, while Sec 4 elaborates on the unique sliding mode control systems. Sec 5 presents simulation results demonstrating the feasibility of the proposed approach. Finally, Sec 6 concludes the paper.

2. Problem Formulation

2.1. Notation

Define that $\mathbb{R}^n$ and $\mathbb{R}$ respectively represent the n-dimensional Euclidean space and real space. For entries $x_1, ..., x_n$, let diag$\{x_1, ..., x_n\}$ stand for the diagonal matrix. Meanwhile, the vector is expressed as $\boldsymbol{x} = [x_1, ..., x_n]^T$. $|\boldsymbol{x}|$ represents the absolute value of $\boldsymbol{x}$, i.e., $|\boldsymbol{x}| = [|x_1|, ..., |x_n|]^T$ and $\|\boldsymbol{x}\|$ denotes the Euclidean norm of $\boldsymbol{x}$, i.e., $\|\boldsymbol{x}\| = \sqrt{\boldsymbol{x}^T\boldsymbol{x}}$. Consider an n-by-n matrix $\boldsymbol{Z}$, its 2-norm is represented as $\|\boldsymbol{Z}\| = \sqrt{\lambda_{\max}(\boldsymbol{Z}^T\boldsymbol{Z})}$. $\lambda_{\max}(\cdot)$ is the maximum eigenvalue. Similarly, $\lambda_{\min}(\cdot)$ is the minimum eigenvalue. $\text{sign}(\boldsymbol{x}) = [\boldsymbol{x}/\|\boldsymbol{x}\|]$ represents the the sign function of the vector $\boldsymbol{x}$. For discontinuous differential equations, we assume that there are Filippov defined solutions[31].
Suppose that a system is represented in the following form:

$$\dot{z} = \boldsymbol{g}(z), \boldsymbol{g}(\boldsymbol{0}) = \boldsymbol{0} \tag{1}$$

where $\boldsymbol{z} = [z_1, .., z_i, \dots z_n]^T \in \mathbb{R}^n$ stands for an n-dimensional state vector and $\boldsymbol{g}(\boldsymbol{z}) = [g_1(\boldsymbol{z}), \dots, g_i(\boldsymbol{z}), \dots g_n(\boldsymbol{z})]^T$ is a known continuous vector field. Based on the system (1), some definitions are presented below.

Definition 1. [32, 33] Consider a vector $\tau = [\tau_1, \dots \tau_i, \dots \tau_n]^T$ with $\tau_i > 0$; then, a mapping $\boldsymbol{z} \to \Lambda_\tau \boldsymbol{z}$ is defined as a dilation, with λ being an arbitrary number and $\Lambda_\tau \boldsymbol{z} = [\lambda^{\tau_1} z_1, \dots, \lambda^{\tau_i} z_i, \dots, \lambda^{\tau_n} z_n]^T$.

Definition 2. [32, 33] If for all $z \in \mathbb{R}^n$, a function $g_i(z) \in R$ satisfies $g_i(\Lambda_\tau z) = \lambda^k g_i(z)$, then for dilation $\Lambda_\tau z$, $g_i(z)$ is considered to be homogeneous with degree $k \in R$. This property can be written as: $\deg(g_i) = k$.

Definition 3. [32, 33] If for all $z \in \mathbb{R}^n$ and any $\lambda > 0$, the following equation holds: $g_i(\Lambda_\tau z) = \lambda^{k+\tau_i} g_i(z)$, then for dilation $\Lambda_\tau z$, the vector $\boldsymbol{g}(z) = [g_1(z), \ldots, g_n(z)]^T$ is considered to be homogeneous with degree k. When this property holds, the system represented by (1) can be considered as being homogeneous.

Lemma 1. *[32, 33] For the system (1), if a Lyapunov function $V(z)$ and real numbers $\ell_1, \ell_2 > 0$, $0 < \ell < 1$ satisfy the conditions below.*

1. *$V(z)$ is constantly positive.*

2. *$\dot{\boldsymbol{V}}(z) + \ell_1 \boldsymbol{V}(z) + \ell_2 \boldsymbol{V}^\ell(z) \leq 0$.*

Then, the system will rapidly converge to the origin, and the convergence time satisfies the following inequality:

$$T(z_0) \leq \frac{1}{\ell_1(1-\ell)} \ln\left(\frac{\ell_2 + \ell_1 \boldsymbol{V}^{1-\ell}(z_0)}{\ell_2}\right) \tag{2}$$

Lemma 2. *[34] Consider time-varying functions ℓ_1 and ℓ_2 in Lemma 1, with $\dot{\ell}_1(t), \dot{\ell}_2(t) > 0$. Given that $\ell_1(t)$ and $\ell_2(t)$ become positive within a finite time, we can deduce $\dot{\boldsymbol{V}}(z) + l_1 \boldsymbol{V}(z) + l_2 \boldsymbol{V}^l(z) \leq 0$ from the aforementioned conditions. Here, l_1 and l_2 are positive real numbers. By invoking the comparison principle [35], the conclusion can be drawn that both $\boldsymbol{V}(z)$ and, consequently, z converge to zero within a finite time. Due to the time-varying nature of $\ell_1(t)$ and $\ell_2(t)$, the precise analysis of the convergence time T_{se} for this observer becomes challenging, as also discussed in [21, 36, 37].*

Definition 4. [38] Consider $\boldsymbol{A}$ and $\boldsymbol{B}$ to be an u × v matrix and a w × t matrix respectively, then the Kronecker product of $\boldsymbol{A}$ and $\boldsymbol{B}$ is expressed as: $\boldsymbol{A} \otimes \boldsymbol{B} = \left[a_{ij}\boldsymbol{B}\right](i = 1, \ldots, u; j = 1, \ldots, v)$, and the result is a partitioned matrix with a dimention $uw \times vt$.

Proposition 1. For a symmetric positive definite matrix $\boldsymbol{Y} = \left[y_{ij}\right](i = 1, \ldots, y; j = 1, \ldots, y) \in \mathbb{R}^{y \times y}$, the matrix $\tilde{\boldsymbol{Y}} = \boldsymbol{Y} \otimes \boldsymbol{I}_{mm} \in \mathbb{R}^{my \times my}$ is symmetric positive definite as well.

Proof. According to the Definition 4, it can be observed that $\tilde{\boldsymbol{Y}} = \left[y_{ij}\boldsymbol{I}_{mm}\right]$. It is easy to prove that $\tilde{\boldsymbol{Y}}$ is a symmetric matrix. Let $\lambda_1, \ldots, \lambda_y$ and $\mu_1, \ldots, \mu_m$ respectively be the eigenvalues of matrices $\boldsymbol{Y}$ and $\boldsymbol{I}_{mm}$, respectively. Hence, the eigenvalues of symmetric matrix $\tilde{\boldsymbol{Y}}$ can be expressed in [38]: $\tau_h = \lambda_o \mu_q (o = 1, \ldots, y, q = 1, \ldots, m; h = 1, \ldots, ym)$.

Because $\boldsymbol{Y}$ and $\boldsymbol{I}_{mm}$ are both positive definite and symmetric, their eigenvalues are both positive. Moreover, $\tilde{\boldsymbol{Y}}$ is positive definite as long as $\zeta_k = \lambda_i \mu_j > 0$. In conclusion, $\tilde{\boldsymbol{Y}}$ is symmetric positive definite. □

2.2. Attitude Dynamics Model

The attitude dynamics model of the Reusable Launch Vehicle (RLV) as presented by [39] is expressed in equations (1) to (6):

$$\begin{aligned}\dot{\alpha} = q - p\cos\alpha\tan\beta - \nu\sin\alpha\tan\beta + \tfrac{\sin\sigma}{\cos\beta}[\dot{\nu}\cos\varphi\dot{\phi}\sin\nu\sin\varphi + (\dot{\rho}+\varpi)\cdot \\ (\cos\phi\cos\nu\sin\varphi - \sin\phi\cos\varphi)] - \tfrac{\cos\sigma}{\cos\beta}[\dot{\varphi} - \dot{\phi}\cos\nu - (\dot{\rho}+\varpi)\cos\phi\sin\nu] + d_1\end{aligned} \tag{3}$$

$$\begin{aligned}\dot{\beta} = p\sin\alpha - \nu\cos\alpha + \sin\sigma[\dot{\varphi} - \dot{\phi}\cos\nu + (\dot{\rho}+\varpi)\cos\phi\sin\nu] + \cos\sigma\cdot \\ [\dot{\nu}\cos\varphi - \dot{\phi}\sin\nu\sin\varphi - (\dot{\rho}+\varpi)(\cos\phi\cos\nu\sin\varphi\sin\phi\cos\varphi)] + d_2\end{aligned} \tag{4}$$

$$\begin{aligned}\dot{\sigma} = -p\cos\alpha\cos\beta - q\sin\beta - \nu\sin\alpha\cos\beta + \dot{\alpha}\sin\beta - \dot{\nu}\sin\varphi \\ -\dot{\phi}\sin\nu\cos\varphi + (\dot{\rho}+\varpi)(\cos\phi\cos\nu\cos\varphi + \sin\phi\sin\varphi) + d_3\end{aligned} \tag{5}$$

$$\dot{p} = \tfrac{I_{zz}M_x}{I_{xx}I_{zz}-I_{xz}^2} + \tfrac{I_{xx}M_z}{I_{xx}I_{zz}-I_{xz}^2} + \tfrac{(I_{xx}-I_{yy}+I_{zz})I_{xz}}{I_{xx}I_{zz}-I_{xz}^2}pq + \tfrac{(I_{yy}-I_{zz})I_{zz}-I_{xz}^2}{I_{xx}I_{zz}-I_{xz}^2}q\nu + d_4 \tag{6}$$

$$\dot{q} = \tfrac{M_y}{I_{yy}} + \tfrac{I_{xz}}{I_{yy}}\left(\nu^2 - p^2\right) + \tfrac{I_{zz}-I_{xx}}{I_{yy}}p\nu + d_5 \tag{7}$$

$$\dot{\nu} = \tfrac{I_{xz}M_x}{I_{xx}I_{zz}-I_{xz}^2} + \tfrac{I_{xx}M_z}{I_{xx}I_{zz}-I_{xz}^2} + \tfrac{(I_{yy}-I_{xx}-I_{zz})I_{xz}}{I_{xx}I_{zz}-I_{xz}^2}q\nu + \tfrac{(I_{xx}-I_{yy})I_{xx}-I_{xz}^2}{I_{xx}I_{zz}-I_{xz}^2}pq + d_6 \tag{8}$$

where the angles of attack, sideslip, and bank are denoted as α, β, and σ, respectively. The roll, pitch, and yaw angular rates of the body-fixed reference frame are represented by p, q, and ν, while the roll, pitch, and yaw moments are denoted as M_x, M_y, and M_z. The moment of inertia for roll, yaw, and pitch are represented by I_{ij}, where i and j correspond to roll, yaw, and pitch moments of inertia. The unknown external disturbances are represented by d_i ($i = 1, \ldots, 6$). The latitude and longitude are denoted as ϕ and ϱ, respectively. Flight path angle and heading angle are represented by φ and ν.

The attitude dynamics of a rigid RLV can be expressed as [40]:

$$\dot{\boldsymbol{\Theta}} = \boldsymbol{\Delta}_f + \boldsymbol{R}\boldsymbol{\omega} \tag{9a}$$

$$\boldsymbol{I}\dot{\boldsymbol{\omega}} = -\boldsymbol{\Omega}\boldsymbol{I}\boldsymbol{\omega} + \boldsymbol{M} + \boldsymbol{I}\boldsymbol{\Delta}_d \tag{9b}$$

In Eq. (9), $\boldsymbol{\Theta} = [\alpha, \beta, \sigma]^T$ and $\boldsymbol{\omega} = [p, q, \nu]^T$. $\boldsymbol{M} = [M_x, M_y, M_z]^T$. $\boldsymbol{\Delta}_f \in \mathbb{R}^3$ and $\boldsymbol{\Delta}_d \in \mathbb{R}^3$ represent the additive disturbances caused by the environmental disturdance and model simplification. Matrix terms $\boldsymbol{R}$, $\boldsymbol{I}$, $\boldsymbol{\Omega} \in \mathbb{R}^{3\times3}$, and $\boldsymbol{\Delta}_M \in \mathbb{R}^3$ are given by:

$$\boldsymbol{\Delta}_M = \boldsymbol{I}\boldsymbol{\Delta}_d = \boldsymbol{I}\begin{bmatrix} d_4 \\ d_5 \\ d_6 \end{bmatrix} = \begin{bmatrix} I_{xx}d_4 - I_{xy}d_5 - I_{xz}d_6 \\ -I_{xy}d_4 - I_{yy}d_5 - I_{yz}d_6 \\ -I_{xz}d_4 - I_{yz}d_5 - I_{zz}d_6 \end{bmatrix} \tag{10}$$

$$\boldsymbol{R} = \begin{bmatrix} -\tan\beta\cos\alpha & 1 & -\tan\beta\sin\alpha \\ \sin\alpha & 0 & -\cos\alpha \\ -\cos\beta\cos\alpha & -\sin\beta & -\cos\beta\sin\alpha \end{bmatrix} \tag{11}$$

$$\boldsymbol{I} = \begin{bmatrix} I_{xx} & 0 & -I_{xz} \\ 0 & I_{yy} & 0 \\ -I_{xz} & 0 & I_{zz} \end{bmatrix}, \boldsymbol{\Omega} = \begin{bmatrix} 0 & -\nu & q \\ \nu & 0 & -p \\ -q & p & 0 \end{bmatrix} \tag{12}$$

In Eq. (12), I_{ij} $(i, j = x, y, z)$ refers to the inertia moments.

For the further explanation of the algorithm, some assumptions are given below.

Assumption 1. All states assumed to be measurable and used for feedback, and the limited range of sideslip angle θ varies from $-(\pi/2)$ to $(\pi/2)$.

Assumption 2. The external disturbances and their first-order derivatives are considered to be limited. That is, $\|\boldsymbol{\Delta}_f\| \leq \eta_1$, $\|\boldsymbol{\Delta}_d\| \leq \eta_2$, $\|\dot{\boldsymbol{\Delta}}_f\| \leq \eta_3$ and $\|\dot{\boldsymbol{\Delta}}_d\| \leq \eta_4$.

Remark 1. The states of RLV can be attained in practice through the inertia navigation system. To prevent the excessive surface temperature in the reentry phase, the sideslip angle θ should be stabilized to zero [39]. Therefore, Assumption 1 is suitable.

2.3. Control Problem Objectives

To have a explicit expression of the control objective, the performance function is defined as below.

Definition 5. [41] If a smooth continuous differential decreasing function $h(t) : \mathbb{R}_+ \to \mathbb{R}_+$ satisfies: $\lim_{t\to\infty} h(t) > 0$, then $h(t)$ is called a performance function.

In this paper, there are two essential control objectives:

- When encountering unknown disturbances $\boldsymbol{\Delta}_f$ and $\boldsymbol{\Delta}_d$, the actual attitude profiles $\boldsymbol{\Theta}$ can follow the objective RLV attitude angle $\boldsymbol{\Theta}_\mathrm{r} = [\alpha_\mathrm{r}, \beta_\mathrm{r}, \sigma_\mathrm{r}]^T$.
- The control objective of this article is to guarantee that the attitude tracking error is confined into a pre-specified region simultaneously, i.e., $e(t) < h(t)$.

To solve the first objective problem, we introduce the follwing tracking error vectors:

$$\boldsymbol{e}_\theta = \boldsymbol{\Theta} - \boldsymbol{\Theta}_\mathrm{r} \tag{13a}$$

$$\boldsymbol{e}_\omega = \boldsymbol{\omega} - \boldsymbol{\omega}_\mathrm{r} \tag{13b}$$

then according to the attitude dynamic system, we can acquire the tracking error dynamics for the two subsystems as below:

$$\dot{\boldsymbol{e}}_\theta = \boldsymbol{R}\boldsymbol{\omega} - \dot{\boldsymbol{\Theta}}_{\mathrm{r}} + \boldsymbol{\Delta}_f \tag{14a}$$

$$\dot{\boldsymbol{e}}_\omega = \boldsymbol{I}^{-1}\boldsymbol{M} - \boldsymbol{I}^{-1}\boldsymbol{\Omega}\boldsymbol{I}\boldsymbol{\omega} - \dot{\boldsymbol{\omega}}_{\mathrm{r}} + \boldsymbol{\Delta}_d \tag{14b}$$

3. Design of the Adaptive Finite-Time Observer(AFO)

In the RLV, the uncertainties affect angular rates and the attitude angles, in the form of disturbance moments and disturbance forces respectively. The control input moments in the angular rate dynamics cannot completely eliminate the unmatched part $\boldsymbol{\Delta}_f$. To solve this problem, this paper redefines the immeasurable state through lumping the unmatched disturbance, and transfers the unmatched problem to observation issue of the RLV error dynamics. The specific error formula is shown in the following formula.

$$\begin{cases} \dot{\boldsymbol{e}}_\theta = \boldsymbol{e}_\omega & (15a) \\ \dot{\boldsymbol{e}}_\omega = -\boldsymbol{R}\boldsymbol{I}^{-1}\boldsymbol{\Omega}(\boldsymbol{\omega})\boldsymbol{I}\boldsymbol{\omega} + \overline{\boldsymbol{M}} - \ddot{\boldsymbol{\theta}}_{\mathrm{r}} + \boldsymbol{\Delta} & (15b) \end{cases}$$

where $\boldsymbol{e}_\theta = \boldsymbol{\Theta} - \boldsymbol{\Theta}_{\mathrm{r}}, \boldsymbol{e}_\omega = \boldsymbol{R}\boldsymbol{\omega} + \boldsymbol{\Delta}_f - \dot{\boldsymbol{\Theta}}_{\mathrm{r}}, \overline{\boldsymbol{M}} = \boldsymbol{R}\boldsymbol{I}^{-1}\boldsymbol{M}$, and $\boldsymbol{\Delta} = \dot{\boldsymbol{R}}\boldsymbol{\omega} + \boldsymbol{R}\boldsymbol{I}^{-1}\boldsymbol{\Delta}_M + \dot{\boldsymbol{\Delta}}_f$. Because of Assumption 2 for the disturbances, $\boldsymbol{\Delta}$ in Eq. (15) satisfies:

Assumption 3. It is presumed that the disturbance $\|\boldsymbol{\Delta}\| \leq L$ and $\|\dot{\boldsymbol{\Delta}}\| \leq L'$, where the constants L and L' are unknown [42].

It can be noted that the error state e_ω is immeasurable due to the unknown disturbance $\boldsymbol{\Delta}_f$. Therefore, a high-performance observer for Eq. (15) is necessary. In the meantime, because $\boldsymbol{\Delta}$ has an unknown upper border, an AFO is better. Here, inspired by Ref. [19], an AFO for Eq. (15) is presented as

$$\dot{\boldsymbol{z}}_1 = -k_1(t)\frac{\boldsymbol{e}_1}{\|\boldsymbol{e}_1\|^{\frac{1}{2}}} - k_2(t)\boldsymbol{e}_1 + \boldsymbol{z}_2 \tag{16a}$$

$$\dot{\boldsymbol{z}}_2 = -k_3(t)\frac{\boldsymbol{e}_1}{\|\boldsymbol{e}_1\|} - k_4(t)\boldsymbol{e}_1 - \boldsymbol{R}\boldsymbol{I}^{-1}\boldsymbol{\Omega}(\boldsymbol{\omega})\boldsymbol{I}\boldsymbol{\omega} + \overline{\boldsymbol{M}} - \ddot{\boldsymbol{\theta}}_{\mathrm{r}} \tag{16b}$$

where the estimation errors are defined as $\boldsymbol{e}_1 = \boldsymbol{z}_1 - \boldsymbol{e}_{\boldsymbol{\theta}}, \boldsymbol{e}_2 = \boldsymbol{z}_2 - \boldsymbol{e}_\omega$. The gains $k_i (i = 1, 2, 3, 4) > 0$ are shown in the following formula:

$$k_1(t) = m_1\sqrt{\chi(t)}, k_2(t) = m_2\chi(t) \tag{17a}$$

$$k_3(t) = m_3\chi(t), k_4(t) = m_4\chi^2(t) \tag{17b}$$

where $m_i (i = 1, 2, 3, 4)$ are positive constants to be defined and χ is a positive, time-varying, scalar function. The parameters m_i are positive constants satisfying

$$9m_1^2m_2^2 + 8m_2^2m_3 < 4m_3m_4 \tag{18}$$

The adaptive law of the time-varying function $\chi(t)$ is given by

$$\dot{\chi}(t) = \begin{cases} \bar{\chi} & \|\boldsymbol{e}_1\| \neq 0 \\ 0 & \|\boldsymbol{e}_1\| = 0 \end{cases} \tag{19}$$

Then, this paper will prove the realizability of the observer reconstruction.

Proof. Substituting Eq. (16) into Eq. (15) yields

$$\dot{\boldsymbol{e}}_1 = -k_1(t)\frac{\boldsymbol{e}_1}{\|\boldsymbol{e}_1\|^{\frac{1}{2}}} - k_2(t)\boldsymbol{e}_1 + \boldsymbol{e}_2 \tag{20a}$$

$$\dot{\boldsymbol{e}}_2 = -k_3(t)\frac{\boldsymbol{e}_1}{\|\boldsymbol{e}_1\|} - k_4(t)\boldsymbol{e}_1 - \boldsymbol{\Delta} \tag{20b}$$

The proof of the realizability of Eq. (16) equals to demonstrating that e_j (j =1, 2) will converge to the origin in finite time. To simplify the analysis, define the vectors below:

$$\boldsymbol{\xi}_1 = \left[\frac{\chi}{\|\boldsymbol{e}_1\|}\right]^{\frac{1}{2}} \boldsymbol{e}_1, \boldsymbol{\xi}_2 = \chi\boldsymbol{e}_1, \boldsymbol{\xi}_3 = \boldsymbol{e}_2 \tag{21}$$

where $\boldsymbol{\xi}_i = [\xi_{i1}, \ldots, \xi_{im}] \in \mathbb{R}^m (i = 1, 2, 3)$. It is noted that when $\boldsymbol{\xi}_i (i = 1, 2, 3) \to 0$ in finite time, $\boldsymbol{e}_j (j = 1, 2) \to 0$ in finite time also stands. Substituting Eq. (21) into Eq. (20) yields

$$\dot{\boldsymbol{e}}_1 = -m_1\boldsymbol{\xi}_1 - m_2\boldsymbol{\xi}_2 + \boldsymbol{\xi}_3 \tag{22}$$

Meanwhile, the following equations can be deduced from Eq. (21):

$$\|\xi_1\| = \left[\frac{\chi}{\|\boldsymbol{e}_1\|}\right]^{\frac{1}{2}} \|\boldsymbol{e}_1\| = [\chi\|\boldsymbol{e}_1\|]^{\frac{1}{2}}, \|\xi_2\| = \chi\|\boldsymbol{e}_1\| \tag{23}$$

We combine Eq. (21) and Eq. (23) to obtain the following formula:

$$\frac{\boldsymbol{e}_1}{\|\boldsymbol{e}_1\|} = \frac{\chi^{\frac{1}{2}\boldsymbol{e}_1}}{\|\boldsymbol{e}_1\|^{\frac{1}{2}}} \frac{1}{[\chi\|\boldsymbol{e}_1\|]^{\frac{1}{2}}} = \frac{\xi_1}{\|\xi_1\|} = \frac{\chi\boldsymbol{e}_1}{\chi\|\boldsymbol{e}_1\|} = \frac{\xi_2}{\|\xi_2\|} \tag{24}$$

Given the Eq. (21) definition, we have the following relationships:

$$\frac{\boldsymbol{e}_1}{\|\boldsymbol{e}_1\|^{\frac{1}{2}}} = \frac{\boldsymbol{\xi}_1}{\chi^{\frac{1}{2}}} \Rightarrow \|\boldsymbol{e}_1\|^{\frac{1}{2}} = \frac{\|\xi_1\|}{\chi^{\frac{1}{2}}} \Rightarrow \left[\frac{\chi}{\|\boldsymbol{e}_1\|}\right]^{\frac{1}{2}} = \frac{\chi}{\|\boldsymbol{\xi}_1\|} \tag{25}$$

The derivative of Eq. (21) results in

$$\dot{\boldsymbol{\xi}}_1 = \left[\frac{\chi}{\|\boldsymbol{e}_1\|}\right]^{\frac{1}{2}} \dot{\boldsymbol{e}}_1 + \frac{[\dot{\chi}\|\boldsymbol{e}_1\|]^{\frac{1}{2}} - [\chi\|\dot{\boldsymbol{e}}_1\|]^{\frac{1}{2}}}{\|\boldsymbol{e}_1\|}\boldsymbol{e}_1 = \left[\frac{\chi}{\|\boldsymbol{e}_1\|}\right]^{\frac{1}{2}} \left[\boldsymbol{I}_{mm} - \frac{\boldsymbol{e}_1\boldsymbol{e}_1^T}{2\|\boldsymbol{e}_1\|^2}\right]\dot{\boldsymbol{e}}_1 + \frac{\bar{\chi}}{2[\chi\|\boldsymbol{e}_1\|]^{\frac{1}{2}}}\boldsymbol{e}_1 \tag{26}$$

$$\dot{\boldsymbol{\xi}}_2 = \bar{\chi}\boldsymbol{e}_1 + \chi\dot{\boldsymbol{e}}_1 \tag{27}$$

$$\dot{\boldsymbol{\xi}}_3 = \dot{\boldsymbol{e}}_2 = -m_3\frac{\chi\boldsymbol{e}_1}{\|\boldsymbol{e}_1\|} - m_4\chi^2\boldsymbol{e}_1 - \dot{\boldsymbol{\Delta}} \tag{28}$$

It is easy to deduce that as $\boldsymbol{\xi}_i (i = 1, 2, 3)$ converges to 0, $\dot{\boldsymbol{\xi}}_i (i = 1, 2, 3)$ also converges to 0, which satisfies the condition of Eq. (1) [32].

For the convenience of subsequent calculation, a new matrix $\boldsymbol{\xi}$ is created as follows:

$$\boldsymbol{\xi} = \begin{bmatrix} \boldsymbol{\xi}_1 \\ \boldsymbol{\xi}_2 \\ \boldsymbol{\xi}_3 \end{bmatrix} \tag{29}$$

here $\boldsymbol{\xi} \in \mathbb{R}^{3m}$ is a $3m$ dimension column ector. Combining Eq. (22) and Eq. (24), the item $\left[\boldsymbol{I}_{mm} - \left(\boldsymbol{e}_1 \boldsymbol{e}_1^T / 2\left\|\boldsymbol{e}_1\right\|^2\right)\right] \dot{\boldsymbol{e}}_1$ (denoted by $\boldsymbol{\Upsilon}$ for brevity) in Eq. (26) can be rewritten as:

$$\boldsymbol{\Upsilon} = \left[\boldsymbol{\xi}_3 - \frac{\boldsymbol{\xi}_1 \boldsymbol{\xi}_1^T \boldsymbol{\xi}_3}{2\left\|\boldsymbol{\xi}_1\right\|^2}\right] - \sum_{i=1}^{2} m_i \left[\boldsymbol{I}_{mm} - \frac{\boldsymbol{\xi}_i \boldsymbol{\xi}_i^T}{2\left\|\boldsymbol{\xi}_i\right\|^2}\right] \boldsymbol{\xi}_i = \boldsymbol{\xi}_3 - \frac{\boldsymbol{\xi}_1 \boldsymbol{\xi}_1^T \boldsymbol{\xi}_3}{2\left\|\boldsymbol{\xi}_1\right\|^2} - \frac{m_1 \boldsymbol{\xi}_1 + m_2 \boldsymbol{\xi}_2}{2} \tag{30}$$

Substituting Eqs. (25) ~ (30) into Eqs. (26) ~ (28) results in

$$\dot{\boldsymbol{\xi}}_1 = \frac{\chi^{\frac{1}{2}} \chi^{\frac{1}{2}}}{\|\boldsymbol{\xi}\|} \left[\boldsymbol{\xi}_3 - \frac{\boldsymbol{\xi}_1 \boldsymbol{\xi}_1^T \boldsymbol{\xi}_3}{2\left\|\boldsymbol{\xi}_1\right\|^2} - \frac{m_1 \boldsymbol{\xi}_1 + m_2 \boldsymbol{\xi}_2}{2}\right] + \frac{\bar{\chi} \boldsymbol{\xi}_1}{2\sqrt{\chi}\sqrt{\chi}} = \frac{\chi}{2\|\boldsymbol{\xi}_1\|}(-m_1 \boldsymbol{\xi}_1 - m_2 \boldsymbol{\xi}_2 + 2\boldsymbol{\xi}_3) + \frac{\bar{\chi} \boldsymbol{\xi}_1}{2\chi} - \frac{\chi \boldsymbol{\xi}_1 \boldsymbol{\xi}_1^T \boldsymbol{\xi}_3}{2\|\boldsymbol{\xi}_1\|^3} \tag{31}$$

$$\dot{\boldsymbol{\xi}}_2 = \frac{\bar{\chi} \boldsymbol{\xi}_2}{\chi} + \chi(-m_1 \boldsymbol{\xi}_1 - m_2 \boldsymbol{\xi}_2 + \boldsymbol{\xi}_3) \tag{32}$$

$$\dot{\boldsymbol{\xi}}_3 = -m_3 \frac{\chi \boldsymbol{\xi}_1}{\left\|\boldsymbol{\xi}_1\right\|} - m_4 \chi^2 \frac{\boldsymbol{\xi}_2}{\chi} - \dot{\boldsymbol{\Delta}} = -\frac{m_3 \chi \boldsymbol{\xi}_1}{\left\|\boldsymbol{\xi}_1\right\|} - m_4 \chi \boldsymbol{\xi}_2 - \dot{\boldsymbol{\Delta}} \tag{33}$$

Expressing Eqs. (31) ~ (33) in matrix form:

$$\dot{\boldsymbol{\xi}} = -\frac{\chi}{2\left\|\boldsymbol{\xi}_1\right\|} \boldsymbol{H}_1 \boldsymbol{\xi} - \chi \boldsymbol{H}_2 \boldsymbol{\xi} + \boldsymbol{H}_3 \tag{34}$$

here $\boldsymbol{H}_1, \boldsymbol{H}_2 \in \mathbb{R}^{3m \times 3m}$ and vector $\boldsymbol{H}_3 \in \mathbb{R}^{3m}$ re calculated as follows:

$$\boldsymbol{H}_1 = \begin{bmatrix} m_1 \boldsymbol{I}_{mm} & m_2 \boldsymbol{I}_{mm} & -2\boldsymbol{I}_{mm} \\ \boldsymbol{0}_{mm} & \boldsymbol{0}_{mm} & \boldsymbol{0}_{mm} \\ 2m_3 \boldsymbol{I}_{mm} & \boldsymbol{0}_{mm} & \boldsymbol{0}_{mm} \end{bmatrix} \tag{35}$$

$$\boldsymbol{H}_2 = \begin{bmatrix} \boldsymbol{0}_{mm} & \boldsymbol{0}_{mm} & \boldsymbol{0}_{mm} \\ m_1 \boldsymbol{I}_{mm} & m_2 \boldsymbol{I}_{mm} & -\boldsymbol{I}_{mm} \\ \boldsymbol{0}_{mm} & m_4 \boldsymbol{I}_{mm} & \boldsymbol{0}_{mm} \end{bmatrix} \tag{36}$$

$$\boldsymbol{H}_3 = \frac{\bar{\chi}}{2\chi} \begin{bmatrix} \boldsymbol{\xi}_1 \\ 2\boldsymbol{\xi}_2 \\ \boldsymbol{0}_m \end{bmatrix} - \begin{bmatrix} \boldsymbol{0}_m \\ \boldsymbol{0}_m \\ \dot{\boldsymbol{\Delta}} \end{bmatrix} - \begin{bmatrix} \frac{\chi \boldsymbol{\xi}_1 \boldsymbol{\xi}_1^T \boldsymbol{\xi}_3}{2\|\boldsymbol{\xi}_1\|^3} \\ \boldsymbol{0}_m \\ \boldsymbol{0}_m \end{bmatrix} \tag{37}$$

To derive that $\boldsymbol{\xi}$ in Eq. (34) converges to zero in finite time, the matrix $\boldsymbol{P} \in \mathbb{R}^{3m \times 3m}$ is designed as

$$\boldsymbol{P} = \begin{bmatrix} \left(4m_3 + m_1^2\right) \boldsymbol{I}_{mm} & m_1 m_2 \boldsymbol{I}_{mm} & -m_1 \boldsymbol{I}_{mm} \\ m_1 m_2 \boldsymbol{I}_{mm} & \left(2m_4 + m_2^2\right) \boldsymbol{I}_{mm} & -m_2 \boldsymbol{I}_{mm} \\ -m_1 \boldsymbol{I}_{mm} & -m_2 \boldsymbol{I}_{mm} & 2\boldsymbol{I}_{mm} \end{bmatrix} \tag{38}$$

and the Lyapunov function is introduced:

$$V = \frac{1}{2}\boldsymbol{\xi}^T \boldsymbol{P}\boldsymbol{\xi} \tag{39}$$

which can be further written as

$$V = 2m_3 \left\|\boldsymbol{\xi}_1\right\|^2 + m_4 \left\|\boldsymbol{\xi}_2\right\|^2 + \frac{1}{2}\left\|\boldsymbol{\xi}_3\right\|^2 + \frac{1}{2}\left\|m_1\boldsymbol{\xi}_1 + m_2\boldsymbol{\xi}_2 - \boldsymbol{\xi}_3\right\|^2 \tag{40}$$

Taking the derivative of V in Eq. (39) yields

$$\dot{V} = -\frac{\chi}{2\left\|\boldsymbol{\xi}_1\right\|}\boldsymbol{\xi}^T \Gamma_1 \boldsymbol{\xi} - \chi \boldsymbol{\xi}^T \Gamma_2 \boldsymbol{\xi} + \tilde{V} \tag{41}$$

where $\Gamma_1 = (1/2)\left(\boldsymbol{H}_1^T \boldsymbol{P} + \boldsymbol{P}\boldsymbol{H}_1\right), \Gamma_2 = (1/2)\left(\boldsymbol{H}_2^T \boldsymbol{P} + \boldsymbol{P}\boldsymbol{H}_2\right)$, and $\tilde{V} = \boldsymbol{\xi}^T \boldsymbol{P}\boldsymbol{H}_3$. Below are details about $\Gamma_1$and Γ_2.

$$\boldsymbol{\Gamma_1} = \begin{bmatrix} 4m_1m_3 + m_1^3 - 2m_1m_3 & m_2m_3 + m_1^2m_2 & -1.5m_1^2 - 2m_3 \\ m_2m_3 + m_1^2m_2 & m_1m_2^2 & -1.5m_1m_2 \\ -1.5m_1^2 - 2m_3 & -1.5m_1m_2 & 2m_1 \end{bmatrix} \otimes \boldsymbol{I}_{mm} \tag{42}$$

$$\boldsymbol{\Gamma_2} = \begin{bmatrix} m_1^2m_2 & m_1m_2^2 + 0.5m_1m_4 & -m_1m_2 \\ m_1m_2^2 + 0.5m_1m_4 & m_2m_4 + m_2^3 & -m_2^2 \\ -m_1m_2 & -m_2^2 & m_2 \end{bmatrix} \otimes \boldsymbol{I}_{mm} \tag{43}$$

For the convenience of future calculation, $\boldsymbol{H}_3$ is divided into three parts:

$$\boldsymbol{H}_{31} = \frac{\bar{\chi}}{2\chi}\begin{bmatrix} \boldsymbol{\xi}_1 \\ 2\boldsymbol{\xi}_2 \\ \boldsymbol{0}_m \end{bmatrix}, \boldsymbol{H}_{32} = \begin{bmatrix} \boldsymbol{0}_m \\ \boldsymbol{0}_m \\ \dot{\boldsymbol{\Delta}} \end{bmatrix}, \boldsymbol{H}_{33} = -\begin{bmatrix} \frac{\chi\boldsymbol{\xi}_1\boldsymbol{\xi}_1^T\boldsymbol{\xi}_3}{2\boldsymbol{\xi}_1^3} \\ \boldsymbol{0}_m \\ \boldsymbol{0}_m \end{bmatrix} \tag{44}$$

It is easily verified that $\boldsymbol{H}_3 = \boldsymbol{H}_{31} + \boldsymbol{H}_{32} + \boldsymbol{H}_{33}$. Denote $\tilde{V}_i = \xi^T \boldsymbol{P}\boldsymbol{H}_{3i} (i = 1, 2, 3)$. Then, $\tilde{V}$ can be expressed as

$$\tilde{V} = \tilde{V}_1 + \tilde{V}_2 + \tilde{V}_3 \tag{45}$$

with

$$\begin{aligned} \tilde{V}_1 =& \frac{\bar{\chi}}{2\chi}\left[(4m_3 + m_1^2)\left\|\boldsymbol{\xi}_1\right\|^2 + 3m_1m_2\boldsymbol{\xi}_1^T\boldsymbol{\xi}_2 - m_1\boldsymbol{\xi}_1^T\boldsymbol{\xi}_3 + 2\left(2m_4 + m_2^2\right)\left\|\boldsymbol{\xi}_2\right\|^2 - 2m_2\boldsymbol{\xi}_2^T\boldsymbol{\xi}_3\right] \\ \tilde{V}_2 =& \left[m_1\boldsymbol{\xi}_1^T + m_2\boldsymbol{\xi}_2^T - 2\boldsymbol{\xi}_3^T\right]\dot{\boldsymbol{\Delta}} \\ \tilde{V}_3 =& -\frac{\chi}{2\left\|\boldsymbol{\xi}_1\right\|^3}\left[\left((4m_3 + m_1^2)\boldsymbol{\xi}_1^T + m_1m_2\boldsymbol{\xi}_2^T - \boldsymbol{\xi}_1\boldsymbol{\xi}_1^T\boldsymbol{\xi}_3\right)\boldsymbol{\xi}_1\boldsymbol{\xi}_1^T\boldsymbol{\xi}_3\right] \\ =& -\frac{\chi}{2\left\|\boldsymbol{\xi}_1\right\|}\left[\left(4m_3 + m_1^2\right)\boldsymbol{\xi}_1^T\boldsymbol{\xi}_3 + \frac{m_1m_2\boldsymbol{\xi}_2^T\boldsymbol{\xi}_1\boldsymbol{\xi}_1^T\boldsymbol{\xi}_3}{\left\|\boldsymbol{\xi}_1\right\|^2} - \frac{m_1\boldsymbol{\xi}_3^T\boldsymbol{\xi}_1\boldsymbol{\xi}_1^T\boldsymbol{\xi}_3}{\left\|\boldsymbol{\xi}_1\right\|^2}\right] \end{aligned} \tag{46}$$

The $\tilde{V}_1$ and $\tilde{V}_2$ satisfy the following inequality:

$$\tilde{V}_1 \leq \frac{\bar{\chi}}{2\chi}\boldsymbol{\xi}^T\tilde{\Gamma}_1\boldsymbol{\xi}, \tilde{V}_2 \leq \sqrt{\left(4 + m_1^2 + m_2^2\right)}\|\dot{\boldsymbol{\Delta}}\|\|\boldsymbol{\xi}\| \tag{47}$$

with $\tilde{\Gamma}_1 = \text{diag}\left(\lambda^1_{\tilde{\Gamma}_1}, \lambda^2_{\tilde{\Gamma}_1}, \lambda^3_{\tilde{\Gamma}_1}\right) \otimes \boldsymbol{I}_{mm}$, where $\lambda^1_{\tilde{\Gamma}_1} = \left(4m_3 + m_1^2 + 1.5m_1m_2 + 0.5m_1\right)$, $\lambda^2_{\tilde{\Gamma}_1} = \left(4m_4 + 2m_2^2 + 1.5m_1m_2 + m_2\right)$, and $\lambda^3_{\tilde{\Gamma}_1} = (0.5m_1 + m_2)$. From the definition in Eq. (21), it can be observed that $\boldsymbol{\xi}_2 = \left\|\boldsymbol{\xi}_1\right\| \boldsymbol{\xi}_1$. Besides, it's easy to prove that

$$\frac{\boldsymbol{\xi}_3^T \boldsymbol{\xi}_1 \boldsymbol{\xi}_1^T \boldsymbol{\xi}_3}{\left\|\boldsymbol{\xi}_1\right\|^2} = \frac{\left(\boldsymbol{\xi}_1^T \boldsymbol{\xi}_3\right)^2}{\left\|\boldsymbol{\xi}_1\right\|^2} \leq \left\|\boldsymbol{\xi}_3\right\|^2 \tag{48}$$

Therefore, the following inequality of the $\tilde{V}_3$ in Eq. (46) holds:

$$\tilde{V}_3 \leq -\frac{\chi}{2\left\|\boldsymbol{\xi}_1\right\|}\left[\left(4m_3 + m_1^2\right)\boldsymbol{\xi}_1^T \boldsymbol{\xi}_3 - m_1\left\|\boldsymbol{\xi}_3\right\|^2\right] - \frac{\chi m_1 m_2}{2}\boldsymbol{\xi}_1^T \boldsymbol{\xi}_3 \tag{49}$$

Next, to simplify the analysis, by combining Eq. (41), Eq. (45) and Eq. (49), the following inequality can be obtained:

$$\dot{V} \leq -\frac{\chi}{2\left\|\boldsymbol{\xi}_1\right\|}\boldsymbol{\xi}^T \tilde{\Gamma}_2 \boldsymbol{\xi} - \chi \boldsymbol{\xi}^T \tilde{\Gamma}_3 \boldsymbol{\xi} + \tilde{V}_1 + \tilde{V}_2 \tag{50}$$

with

$$\begin{aligned} \tilde{\Gamma}_2 &= \begin{bmatrix} m_1^3 + 2m_1m_3 & 0 & -m_1^2 \\ 0 & 5m_1m_2^2 + 2m_1m_4 & -3m_1m_2 \\ -m_1^2 & -3m_1m_2 & m_1 \end{bmatrix} \otimes \boldsymbol{I}_{mm} \\ \tilde{\Gamma}_3 &= \begin{bmatrix} 2m_1^2m_2 + m_2m_3 & 0 & 0 \\ 0 & m_2^3 + m_2m_4 & -m_2^2 \\ 0 & -m_2^2 & m_2 \end{bmatrix} \otimes \boldsymbol{I}_{mm} \end{aligned} \tag{51}$$

According to Proposition 1, it can be derived that matrices $\tilde{\Gamma}_2$ and $\tilde{\Gamma}_3$ are positive definite as long as Eq. (18) holds. Consider positive matrices $\tilde{\Gamma}_i (i = 1, 2, 3)$, the following inequalities for any vectors $\boldsymbol{\xi}$ holds:

$$\lambda_{\min}\left(\tilde{\Gamma}_i\right)\|\boldsymbol{\xi}\|^2 \leq \boldsymbol{\xi}^T \tilde{\Gamma}_i \boldsymbol{\xi} \leq \lambda_{\max}\left(\tilde{\Gamma}_i\right)\|\boldsymbol{\xi}\|^2 \tag{52}$$

Equivalently, consider the positive matrix $\boldsymbol{P}$ in Eq. (41), we have $\lambda_{\min}(\boldsymbol{P})\|\xi\|^2 \leq 2V \leq \lambda_{\max}(\boldsymbol{P})\|\xi\|^2$. Consequently, the following condition holds:

$$\frac{\lambda_{\min}\left(\tilde{\Gamma}_i\right)2V}{\lambda_{\max}(\boldsymbol{P})} \leq \boldsymbol{\xi}^T \tilde{\Gamma}_i \boldsymbol{\xi} \leq \frac{\lambda_{\max}\left(\tilde{\boldsymbol{\Gamma}}_i\right)2V}{\lambda_{\min}(\boldsymbol{P})} \tag{53}$$

Substituting Eq. (47) and Eq. (53) into Eq. (50) yields

$$\dot{V} \leq \left[\frac{\bar{\chi}\lambda_{\max}\left(\tilde{\Gamma}_1\right)}{\chi\lambda_{\min}(\boldsymbol{P})} - \frac{2\chi\lambda_{\min}\left(\tilde{\Gamma}_3\right)}{\lambda_{\max}(\boldsymbol{P})}\right]V - \frac{\chi\lambda_{\min}\left(\tilde{\Gamma}_2\right)}{\left\|\boldsymbol{\xi}_1\right\|\lambda_{\max}(\boldsymbol{P})}V + \sqrt{\left(4 + m_1^2 + m_2^2\right)}\|\dot{\boldsymbol{\Delta}}\|\|\boldsymbol{\xi}\| \tag{54}$$

According to Assumption 3, it can be noted that$\|\dot{\boldsymbol{\Delta}}\| \leq C'$. Meanwhile, it is easy to prove that

$$\left\|\boldsymbol{\xi}_1\right\| \leq \|\boldsymbol{\xi}\|, \sqrt{\frac{2V}{\lambda_{\max}(\boldsymbol{P})}} \leq \|\boldsymbol{\xi}\| \leq \sqrt{\frac{2V}{\lambda_{\min}(\boldsymbol{P})}} \tag{55}$$

$\dot{V}$ in Eq. (54) satisfies

$$\dot{V} \leq -\left[\chi\vartheta_2 - \frac{\dot{\chi}}{\chi}\vartheta_1\right]V - \left[\chi\vartheta_3 - \vartheta_4 C'\right]V^{\frac{1}{2}} \tag{56}$$

with constants

$$\begin{cases} \vartheta_1 = \dfrac{\lambda_{\max}\left(\tilde{\Gamma}_1\right)}{\lambda_{\min}(\boldsymbol{P})} & (57a) \\ \vartheta_2 = \dfrac{2\lambda_{\min}\left(\tilde{\Gamma}_3\right)}{\lambda_{\max}(\boldsymbol{P})} & (57b) \\ \vartheta_3 = \dfrac{\lambda_{\min}\left(\tilde{\Gamma}_2\right)\sqrt{\lambda_{\min}(\boldsymbol{P})}}{\sqrt{2}\lambda_{\max}(\boldsymbol{P})} & (57c) \\ \vartheta_4 = \sqrt{\dfrac{8+2m_1^2+2m_2^2}{\lambda_{\min}(\boldsymbol{P})}} & (57d) \end{cases}$$

Because $\dot{\chi} = \overline{\chi} \geq 0$, it is easily found that in finite time $\ell_1 = \chi\vartheta_2 - (\bar{\chi}/\chi)\vartheta_1$ and $\ell_2 = \chi\vartheta_3 - \vartheta_4 C'$ are positive($\dot{\ell}_1 = \overline{\chi}\vartheta_2 + \vartheta_1/\chi^2 > 0, \dot{\ell}_2 = \overline{\chi}\vartheta_3 > 0$). In consideration of Lemma 2 , the vector $\boldsymbol{\xi}$ will converge to $\mathbf{0}$ in finite time. □

Remark 2. In contrast to the approach presented in [34], this paper introduces a novel multi-variable control scheme for the error observer. Through the expressions in Eq. (16), it becomes evident that discontinuities occur only when all components of e_{1i} simultaneously equal zero, where e_{1i} represents the error components (for $i = 1, 2, 3$). Conversely, when utilizing the single variable disturbance observer, any individual component e_{1i} being zero leads to discontinuity. Consequently, the proposed structure exhibits superior chattering reduction capabilities compared to the single variable disturbance observer scheme.

Remark 3. In the development of the error observer for this paper, the knowledge of the upper limit of uncertainty and its gradient is not required during the design process. Since $\ell_1$and ℓ_2 vary with time, analyzing the accurate convergence time for this observer is difficult. According to Lemma 1, $T(z_0)$ (convergence time) can be estimated which is relatively short. To enhance the convergence speed of the observer when the estimation error trajectories deviate significantly from the origin, the introduction of the linear terms $-k_2(t)e_1$ and $-k_4(t)e_1$ is employed. Consequently, the observer equation can be directly utilized for subsequent analysis.

4. Design of the Adaptive Multivariable Algorithm

4.1. Adaptive Multivariable Algorithm Design

Before introducing the proposed algorithm, consider the system as below:

$$\dot{y}_1 = y_2, \dot{y}_2 = u + \boldsymbol{\Delta}_1, y_1(0) = y_{10}, y_2(0) = y_{20} \tag{58}$$

where $y_1 = [y_{11}, ..., y_{1n}]^T$ and $y_2 = [y_{21}, ..., y_{2n}]^T \in \boldsymbol{R}^n$ are the state vectors. $u, \boldsymbol{\Delta}_1(t) \in \boldsymbol{R}^n$ are respectively the control vector and the external disturbance vector. Based on Assumption 3, the inequality of $\boldsymbol{\Delta}_1(t)$ holds: $\|\boldsymbol{\Delta}_1(t)\| \leq \boldsymbol{L}_1$, where $\boldsymbol{L}_1$ is constant but unknown and satisfies $\boldsymbol{L}_1 > 0$. The next theorem shows the conclusion of this section.

Theorem 1. *For the system Eq. (58), the controller below is designed:*

$$u = -y_2 - \frac{\|\boldsymbol{s}\|}{\varepsilon + \|\epsilon_0\|e^{-t} - \|\boldsymbol{s}\|} sign(\boldsymbol{s}) \tag{59}$$

where ε is a random positive constant, ε is a random positive constant satisfying $\|\epsilon_0\| = \varepsilon_1 + \|s_0\|$, and $\boldsymbol{s}$ is the sliding manifold, with $\boldsymbol{s}_0$ being the initial value of $\boldsymbol{s}$. Then, the states y_1 and y_2 will be restricted to the pre-specified regions

$$\begin{cases} \|y_1\| < \varepsilon + (\|y_{10}\| - \varepsilon)e^{-t} + \|\epsilon_0\|te^{-t} & \text{(60a)} \\ \|y_2\| < 2\varepsilon + (\|y_{10}\| - \varepsilon + \|\epsilon_0\|)e^{-t} + \|\epsilon_0\|te^{-t} & \text{(60b)} \end{cases}$$

According to Eq. (60), $\boldsymbol{s}$ will be defined by

$$\boldsymbol{s} = y_1 + y_2 \tag{61}$$

Then, the sliding manifold $\boldsymbol{s}$ will be restricted to the pre-specified region

$$\|\boldsymbol{s}\| < \|\epsilon_0\|e^{-t} + \varepsilon \tag{62}$$

Proof. By Eq. (58) and Eq. (61), the derivative of $\boldsymbol{s}$ with respect to time in can be derived as

$$\dot{\boldsymbol{s}} = \boldsymbol{\Delta}_1(t) + y_2 + u \tag{63}$$

Substituting control law Eq. (59) into Eq. (63), we can get:

$$\dot{\boldsymbol{s}} = -\frac{\|\boldsymbol{s}\| sign(\boldsymbol{s})}{\|\epsilon_0\|e^{-t} + \varepsilon - \|\boldsymbol{s}\|} + \boldsymbol{\Delta}_1(t) \tag{64}$$

Hence, the following two parts will be mainly proved:

(1) it will be demonstrated that $\boldsymbol{s}$ in Eq. (61) would remain in the pre-specified region Eq. (62).

(2) it will be shown that y_1 and y_2 would never escape from the prescribed Eq. (60).

Step 1. *To prove the first part, we propose the Lyapunov function as below:*

$$\boldsymbol{V} = \frac{1}{2}\left[-\boldsymbol{s}^T\boldsymbol{s} + \left(\underbrace{\frac{\|\boldsymbol{s}\|}{\varepsilon + \|\epsilon_0\|e^{-t} - \|\boldsymbol{s}\|}}_{Z(s,t)}\right)^2\right] \tag{65}$$

For the convenience of subsequent calculation, $Z(\boldsymbol{s}, t)$ in Eq. (65) is replaced by Z. The derivative of $\boldsymbol{V}$ with respect to time in Eq. (65) along system (58)-(61) is denoted by

$$\dot{\boldsymbol{V}} = \boldsymbol{s}^T(\boldsymbol{\Delta}_1(t) - Zsign(\boldsymbol{s})) + Z * \frac{\frac{\dot{\boldsymbol{s}}\boldsymbol{s}^T}{\|\boldsymbol{s}\|}(\varepsilon - \|\boldsymbol{s}\| + \|\epsilon_0\|e^{-t}) + \|\boldsymbol{s}\|\left(\frac{\boldsymbol{s}\dot{\boldsymbol{s}}^T}{\|\boldsymbol{s}\|} + \|\epsilon_0\|e^{-t}\right)}{(\varepsilon + \|\epsilon_0\|e^{-t} - \|\boldsymbol{s}\|)^2} \tag{66}$$

Taking into account the fact that $\boldsymbol{s}^T sign(\boldsymbol{s}) = \|\boldsymbol{s}\|$ and Eq. (63), Eq. (66) can be expressed as

$$\dot{\boldsymbol{V}} = \boldsymbol{s}^T(\boldsymbol{\Delta}_1(t) - Zsign(\boldsymbol{s})) + Z * \frac{\varepsilon\left(\frac{\boldsymbol{s}^T\boldsymbol{\Delta}_1}{\|\boldsymbol{s}\|} - Z\right) + \|\epsilon_0\|e^{-t}\left(\frac{\boldsymbol{s}^T\boldsymbol{\Delta}_1}{\|\boldsymbol{s}\|} + \|\boldsymbol{s}\| - Z\right)}{\left(\|\epsilon_0\|e^{-t} + \varepsilon - \|\boldsymbol{s}\|\right)^2} \tag{67}$$

Noting that $\|\boldsymbol{\Delta}_1(t)\| \leq \boldsymbol{L}_1$*, we get*

$$\dot{V} \leq (Z - \boldsymbol{L}_1)\|\boldsymbol{s}\| - \frac{|Z|\left(\varepsilon Z - \varepsilon \boldsymbol{L}_1 - \|\epsilon_0\| e^{-t} \boldsymbol{L}_1\right)}{\left(\varepsilon + \|\epsilon_0\| e^{-t} - \|\boldsymbol{s}\|\right)^2} - \frac{|Z\|\epsilon_0| e^{-t}(Z - \|\boldsymbol{s}\|)}{\left(\varepsilon + \|\epsilon_0\| e^{-t} - \|\boldsymbol{s}\|\right)^2} \tag{68}$$

For simplicity, the functions below are defined:

$$\boldsymbol{G}_1(\|\boldsymbol{s}\|) = Z - \boldsymbol{L}_1 \tag{69a}$$

$$\boldsymbol{G}_2(\|\boldsymbol{s}\|) = \varepsilon (Z - \boldsymbol{L}_1) - \|\epsilon_0\| e^{-t} \boldsymbol{L}_1 \tag{69b}$$

$$\boldsymbol{G}_3(\|\boldsymbol{s}\|) = Z - \|\boldsymbol{s}\| \tag{69c}$$

Thus, Eq. (68) is rewritten as

$$\dot{V} \leq -\|\boldsymbol{s}\| \boldsymbol{G}_1(\|\boldsymbol{s}\|) - \frac{|Z|\boldsymbol{G}_2(\|\boldsymbol{s}\|) - |Z\|\epsilon_0| e^{-t} \boldsymbol{G}_3(\|\boldsymbol{s}\|)}{\left(\varepsilon + \|\epsilon_0\| e^{-t} - \|\boldsymbol{s}\|\right)^2} \tag{70}$$

It can be demonstrated that $\boldsymbol{G}_1(\|\boldsymbol{s}\|)$*,* $\boldsymbol{G}_2(\|\boldsymbol{s}\|)$*, and* $\boldsymbol{G}_3(\|\boldsymbol{s}\|)$ *are strictly positive in the region* $\Xi_1 = \{\boldsymbol{s} \in \boldsymbol{R}^n : \varepsilon < \|\boldsymbol{s}\| < \|\epsilon_0\| e^{-t} + \varepsilon\}$*, where* ε_0 *is a positive number. By solving* $\boldsymbol{G}_2(\|\boldsymbol{s}_1\|) = 0$*, one can get*

$$\|\boldsymbol{s}_1\| = \frac{\boldsymbol{L}_1(\varepsilon + \|\epsilon_0\| e^{-t})}{\varepsilon + \boldsymbol{L}_1(\varepsilon + \|\epsilon_0\| e^{-t})}(\varepsilon + \|\epsilon_0\| e^{-t}) < \|\epsilon_0\| e^{-t} + \varepsilon \tag{71}$$

Notice that $\boldsymbol{G}_2(\|\boldsymbol{s}\|)$ *is positively correlated to* $\|\boldsymbol{s}\|$*. Thus, when* $(\|\boldsymbol{s}_1\| < \|\boldsymbol{s}\| < \varepsilon + \|\epsilon_0\| e^{-t})$*,* $\boldsymbol{G}_2(\|\boldsymbol{s}\|) > \boldsymbol{G}_2(\|\boldsymbol{s}_1\|) = 0$*. From Eq. (69), it follows that* $\boldsymbol{G}_1(\|\boldsymbol{s}\|)$ *and* $\boldsymbol{G}_2(\|\boldsymbol{s}\|)$ *must be both positive. Therefore, when* $\|\boldsymbol{s}\| \in (\|\boldsymbol{s}_1\|, \varepsilon + \|\epsilon_0\| e^{-t})$*,* $\boldsymbol{G}_1(\|\boldsymbol{s}\|)$ *and* $\boldsymbol{G}_2(\|\boldsymbol{s}\|)$ *are both positive.*

Identically, it is easily proved that when $\|\boldsymbol{s}\| \in (\varepsilon - 1 + \|\epsilon_0\| e^{-t}, \varepsilon + \|\epsilon_0\| e^{-t})$*,* $\boldsymbol{G}_3(\|\boldsymbol{s}\|) > 0$*. Select* $\gamma_0 = max(\|\boldsymbol{s}_1\|, \varepsilon - 1 + \|\varepsilon_0\| e^{-t})$*, which ensures that* $\boldsymbol{G}_1(\|\boldsymbol{s}\|)$*,* $\boldsymbol{G}_2(\|\boldsymbol{s}\|)$*, and when* $\|\boldsymbol{s}\| \in (\gamma_0, \varepsilon + \|\epsilon_0\| e^{-t})$*,* $\boldsymbol{G}_3(\|\boldsymbol{s}\|)$ *are positive.*

This means that $\dot{\boldsymbol{V}}$ *in Eq. (68) is strictly negative. It is easy to prove that* $\boldsymbol{V}$ *in Eq. (65) is positively correlated to* $\|\boldsymbol{s}\|$*. Therefore, as soon as* $\|\boldsymbol{s}\|$ *grows and exceeds the border of* γ_0*,* $\dot{\boldsymbol{V}} < 0$ *and* $\boldsymbol{V}$ *decrease, resulting that* $\|\boldsymbol{s}\|$ *decreases. Additionally, it follows from Eq. (66) that when* $\|\boldsymbol{s}\|$ *approaching the border* ε*,* $\dot{\boldsymbol{V}}$ *will also approach negative infinity, making the decrease rate of* $\|\boldsymbol{s}\|$ *go to infinity. It indicates that* $\|\boldsymbol{s}\|$ *reducees faster than* $\|\epsilon_0\| e^{-t}$ *and it will remain in the pre-specified performance region* $\Xi_2 = \{\boldsymbol{s} \in \boldsymbol{R}^n : \|\boldsymbol{s}\| < \varepsilon + \|\epsilon_0\| e^{-t}\}$*.*

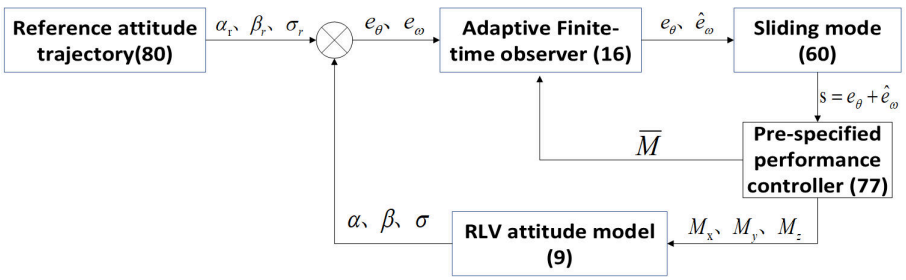

Figure 1: Schematic diagram of the entire system

Step 2. *Consider the following Lyapunov function:*

$$\boldsymbol{V}_1 = \|x_1\| \tag{72}$$

Bearing in mind $\boldsymbol{s} = x_1 + x_2$ *, the derivative of* $\boldsymbol{V}_1$ *with respect to time along Eq. (58) is given as follows:*

$$\dot{\boldsymbol{V}}_1 = \frac{x_1^T(-x_1 + \boldsymbol{s})}{\|x_1\|} \leq -\|x_1\| + \|\boldsymbol{s}\| \tag{73}$$

Taking into account Eq. (72) and Eq. (62), the upper boundary of $\dot{\boldsymbol{V}}_1$ *in Eq. (73) satisfies the following inequality:*

$$\dot{\boldsymbol{V}}_1 < -\boldsymbol{V}_1 + \varepsilon + \|\epsilon_0\|e^{-t} \tag{74}$$

By integrating both sides of Eq. (74), one can get

$$\boldsymbol{V}_1 \leq \varepsilon + (\boldsymbol{V}_1(0) - \varepsilon)e^{-t} + \|\epsilon_0\|te^{-t} \tag{75}$$

Substituting Eq. (72) into Eq. (75), Eq. (60a) can be proved.

Moreover, $\|x_2\| = \| - x_1 + \boldsymbol{s}\| \leq \|x_1\| + \|\boldsymbol{s}\| < 2\varepsilon + (\|\epsilon_0\| + \|x_{10}\| - \varepsilon)e^{-t} + \|\epsilon_0\|te^{-t}$.

□

Remark 4. The adaptive gain of the proposed governing law Eq. (59) can be indicated as $Z(\boldsymbol{s}, t)$, which is defined in the equation (65). It can be noted that the value of $Z(\boldsymbol{s}, t)$ is determined by the sliding manifold $\boldsymbol{s}$. With $\boldsymbol{s}$ monotonically approaching zero, $Z(\boldsymbol{s}, t)$ will consequently approach zero.

Remark 5. The present algorithm is based on the work introduced in [43]. In comparison with [43], the developed multivariable controller (59) in this paper incorporates an exponential decay time-varying term, leading to several improvements. Firstly, unlike in [43], the present work eliminates the need for a detection mechanism to determine the time instant when the sliding manifold enters a neighborhood of zero. This is particularly advantageous in the presence of imperfections such as sampling step and sampling noise, where accurate detection can be challenging. By avoiding the need for a detection mechanism, the proposed approach simplifies the implementation process. Secondly, the developed controller in this work not only guarantees steady-state performance but also ensures desirable transient behavior of the closed-loop systems. In contrast, [43] only addresses steady-state performance. By considering transient response, the proposed controller enables improved system behavior and enhances overall performance. Lastly, it is important to highlight that the proposed controller is designed for multivariable systems, while the controller in [43] is applicable only to scalar systems. This extension to the multivariable domain allows for broader application of the proposed controller and expands its capabilities in handling complex systems. Therefore, the algorithm designed in this paper has a better chattering attenuation effect than [43].

4.2. Application to Attitude Control of RLV

According to Eq. (15,16), this paper uses the new error system generated by the observer to construct a new error model as follows:

$$\dot{e}_\theta = \widehat{e_\omega} - e_2 \tag{76a}$$

$$\dot{\widehat{e}}_\omega = \underbrace{-\boldsymbol{R}\boldsymbol{I}^{-1}\boldsymbol{\Omega}\boldsymbol{I}\boldsymbol{\omega} - \ddot{\boldsymbol{\theta}}_r}_{\boldsymbol{F}} + \underbrace{\boldsymbol{R}\boldsymbol{I}^{-1}\boldsymbol{M}}_{\boldsymbol{M}'} + \underbrace{\boldsymbol{R}\boldsymbol{I}^{-1}\boldsymbol{\Delta}_{\boldsymbol{M}} + \dot{\boldsymbol{\Delta}}_f + \dot{\boldsymbol{R}}\boldsymbol{\omega} + \dot{e}_2}_{\boldsymbol{\Delta}'(t)} \tag{76b}$$

According to Assumption 3, the disturbance $\boldsymbol{\Delta}'(t)$ in Eq. (76) satisfies the inequality below:

$$\|\boldsymbol{\Delta}'(t)\| \leq \boldsymbol{L} \tag{77}$$

where $\boldsymbol{L}$ is a constant. Hence, based on Theorem 1, PSMC for the attitude error system described as Eq. (76) can be designed, which will be illustrated in detail.

Theorem 2. *Consider system Eq. (76) with the controller*

$$\boldsymbol{M}' = -\widehat{e_\omega} - \boldsymbol{F} - \frac{\|\boldsymbol{s}\|}{\varepsilon + \|\epsilon_0\|e^{-t} - \|\boldsymbol{s}\|}\, sign(\boldsymbol{s}) \tag{78}$$

where the sliding mode vector $s = e_\theta + \widehat{e_\omega}$, ε is a random positive number, and $\|\epsilon_0\| = \varepsilon_1 + \|s_0\|$, where ε_1 is a non-negative number. According to Eq. (60) and Eq. (62), we can get the following pre-specified performance region that limits s and attitude tracking errors :

$$\begin{cases} \|e_\theta\| < \varepsilon + (\|e_{10}\| - \varepsilon)e^{-t} + \|\epsilon_0\|te^{-t} & (79a) \\ \|\widehat{e_\omega}\| < 2\varepsilon + (\|\epsilon_0\| + \|e_{10}\| - \varepsilon)e^{-t} + \|\epsilon_0\|te^{-t} & (79b) \\ \|s\| < \varepsilon + \|\epsilon_0\|e^{-t} & (79c) \end{cases}$$

According to Eq. (76), the real control $\boldsymbol{M}$ can be calculated by $\boldsymbol{M} = \boldsymbol{I}\boldsymbol{R}^{-1}\boldsymbol{M}'$.

Proof. According to Remark 2, when designing the controller in this experiment, control is carried out after the observer of the former reaches the convergence time T_{ob}, that is, e_2 will converge to the origin. So Eq. (76) becomes:

$$\dot{e}_\theta = \widehat{e_\omega} \tag{80a}$$

$$\dot{\widehat{e}}_\omega = \underbrace{-\boldsymbol{R}\boldsymbol{I}^{-1}\boldsymbol{\Omega}\boldsymbol{I}\boldsymbol{\omega} - \ddot{\boldsymbol{\theta}}_r}_{\boldsymbol{F}} + \underbrace{\boldsymbol{R}\boldsymbol{I}^{-1}\boldsymbol{M}}_{\boldsymbol{M}'} + \underbrace{\boldsymbol{R}\boldsymbol{I}^{-1}\boldsymbol{\Delta}_{\boldsymbol{M}} + \dot{\boldsymbol{\Delta}}_f + \dot{\boldsymbol{R}}\boldsymbol{\omega} + \dot{e}_2}_{\boldsymbol{\Delta}'(t)} \tag{80b}$$

Note that the acknowledged term $\boldsymbol{F}$ in Eq. (80) can be seen as the nominal part of the system, which can be offset through the proposed control in Eq. (78). Hence, Theorem 2 can be deducted from Theorem 1. □

5. Simulation

The inertia moments are given as: $I_{xx} = 434270kg \cdot m^2$, $I_{xz} = 17880kg \cdot m^2$, $I_{yy} = 961220kg \cdot m^2$, and $I_{zz} = 1131541kg \cdot m^2$. Additionally, assuming that the inertia matrix has some uncertainty, we set $\boldsymbol{I} = \boldsymbol{I} + \Delta\boldsymbol{I}$ with $\Delta\boldsymbol{I} = 0.05\boldsymbol{I}$ .The guidance command $\boldsymbol{\Theta_r}$ is obtained from the literature [30]:

$$\boldsymbol{\Theta_r} = \begin{bmatrix} 0.5sin(t) \\ 0.4cos(t) \\ 0.3sin(t) \end{bmatrix} rad \tag{81}$$

Initial angles and angular rates are selected as

$$\boldsymbol{\Theta}(0) = \begin{bmatrix} 0.2 \\ 0.2 \\ 0.2 \end{bmatrix} rad, \boldsymbol{\omega}(0) = \begin{bmatrix} 0 \\ 0 \\ 0 \end{bmatrix} rad/s \tag{82}$$

The PSMC parameters are taken as $\varepsilon = 0.01$ and $\varepsilon_1 = 0$. The parameters of the AFO are set as $m_1 = m_2 = 0.3$, $m_3 = m_4 = 0.5, \chi = 10, \chi_s = 0.01$. We set the sampling time of simulation to be 1 ms.

To demonstrate the effectiveness of the proposed approach in disturbance suppression, disturbances are sequentially introduced in the following manner: In this simulation, the disturbances are :

$$\boldsymbol{\Delta}_f = \begin{cases} 0 & t < 10 \\ \begin{bmatrix} \frac{3}{10} sin\frac{3t}{2} \\ 1 + \frac{3}{10} cos\frac{3t}{2} \\ \frac{3}{10}(1 + sin\frac{3t}{2} + cos\frac{3t}{2}) \end{bmatrix} & t > 10 \end{cases}, \boldsymbol{\Delta}_M = \begin{bmatrix} \frac{3}{10} sin\frac{3t}{2} \\ 1 + \frac{3}{10} cos\frac{3t}{2} \\ \frac{3}{10}\left(1 + sin\frac{3t}{2} + cos\frac{3t}{2}\right) \end{bmatrix} \times 10^6 \tag{83}$$

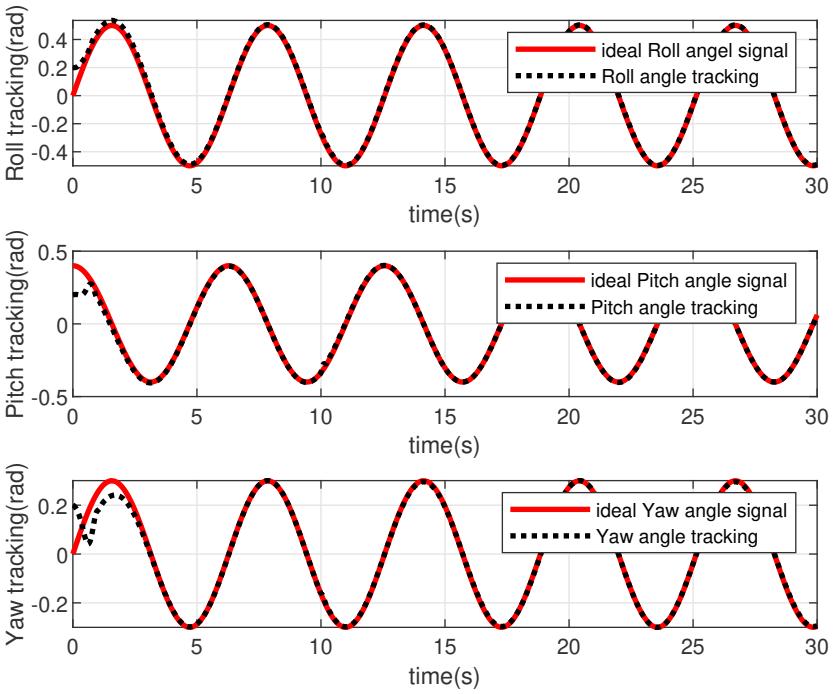

Figure 2: Attitude tracking

Fig. 2 shows the attitude tracking curves of the proposed system. The developed controller can effectively track the reference signals, which can be deducted from Fig. 2.

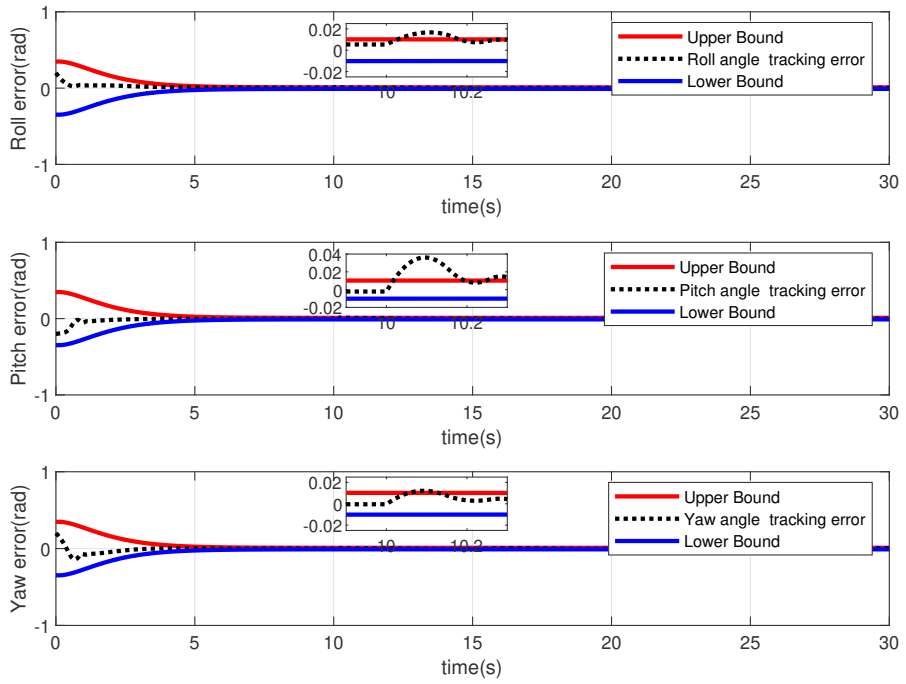

Figure 3: Attitude tracking errors

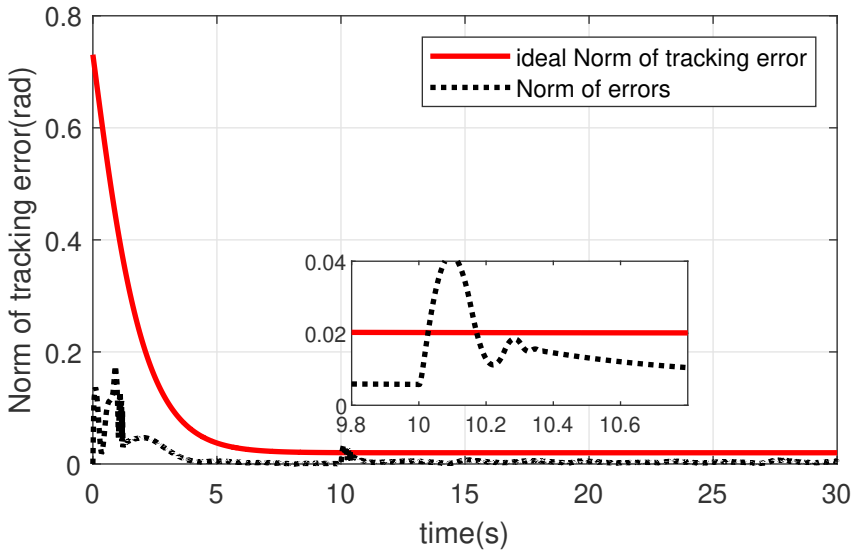

Figure 4: Norm of attitude tracking errors

Figs. 3 and 4 provide the attitude tracking errors and the norm of the errors respectively. It can be seen from the results that the errors and their norm are limited within the pre-specified performance range defined by (79). By adding mismatched disturbances in t=10, it can be seen that the system quickly converges the attitude tracking error to the specified region. Fig. 4 displays the norm of attitude tracking errors, and the details at t=10 is displayed in the

zoomed figures of Fig. 4. And by the tuning parameter ε in (78) the accuracy can be set in advance.

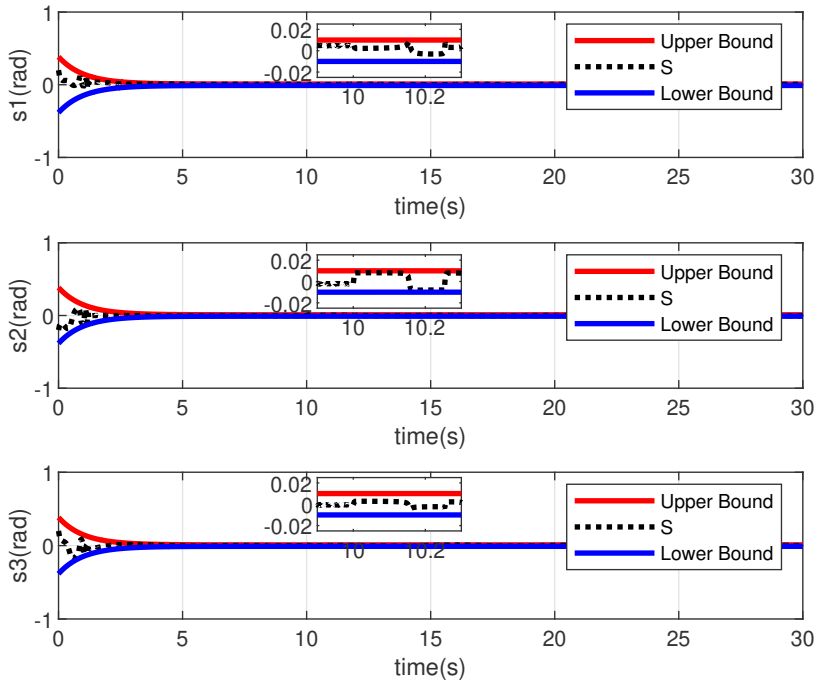

Figure 5: Sliding mode manifold

Fig. 5 shows how every dimension of the sliding mode manifold s evolves. From Fig. 5, it is easy to find that s will be restricted within the pre-specified performance range defined by Eq. (79).

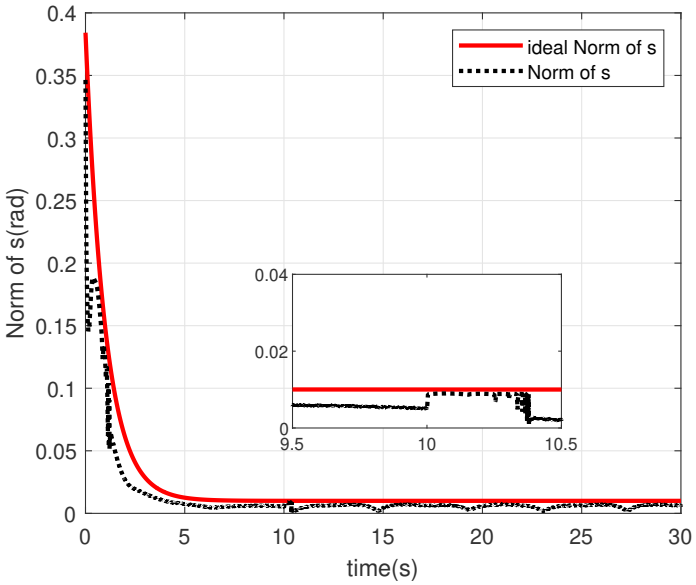

Figure 6: Norm of the sliding manifold

Additionally, Fig. 6 shows the norm of s and its pre-specified performance region(s).

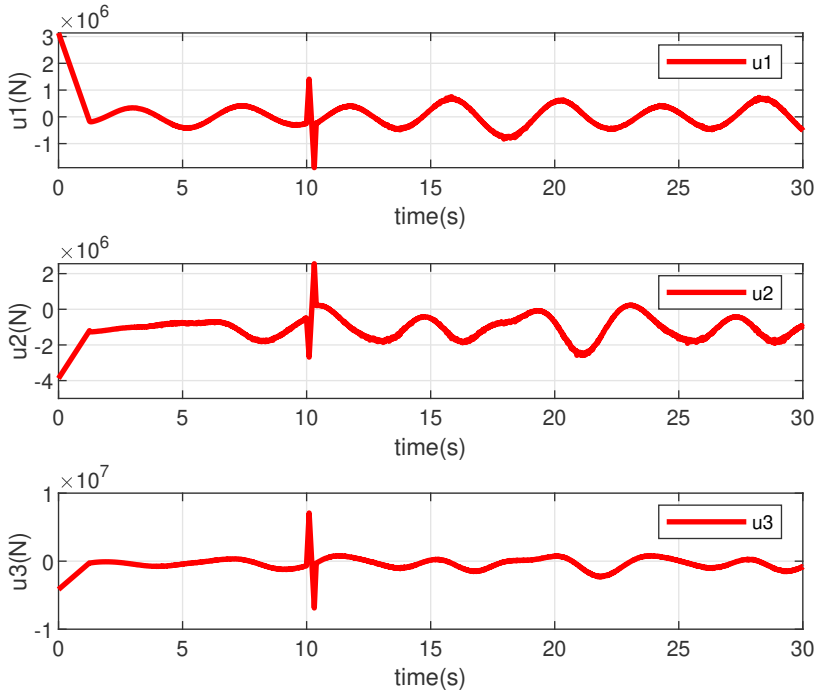

Figure 7: Attitude control signal

In addition, Fig. 7 shows the attitude control signals as well as the availability of the proposed controller.

To showcase the superiority of our designed algorithm (AFO-ASMC), we compare our approach with the ASMC method from [5]. Both methods utilize parameters consistent with those employed previously. The simulation results are illustrated in the figure below:

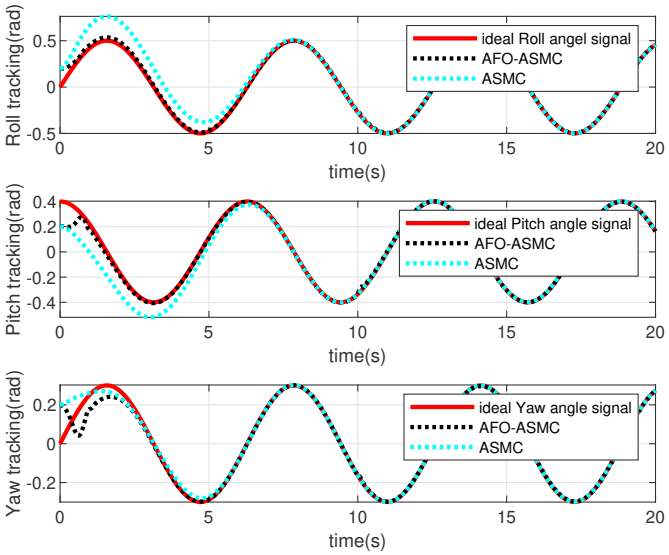

Figure 8: Attitude tracking errors

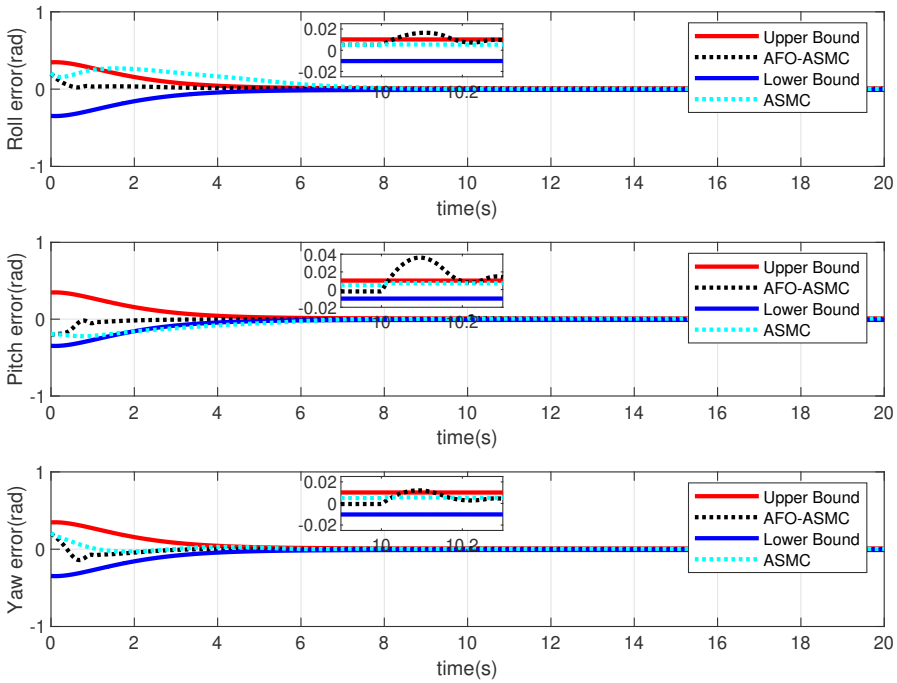

Figure 9: Attitude tracking errors

Fig. 8 shows the attitude tracking curves of two methods. From Fig. 8, it is evident that the convergence rate of

AFO-SMC is faster than that of ASMC. Fig. 9 provides the attitude tracking errors.

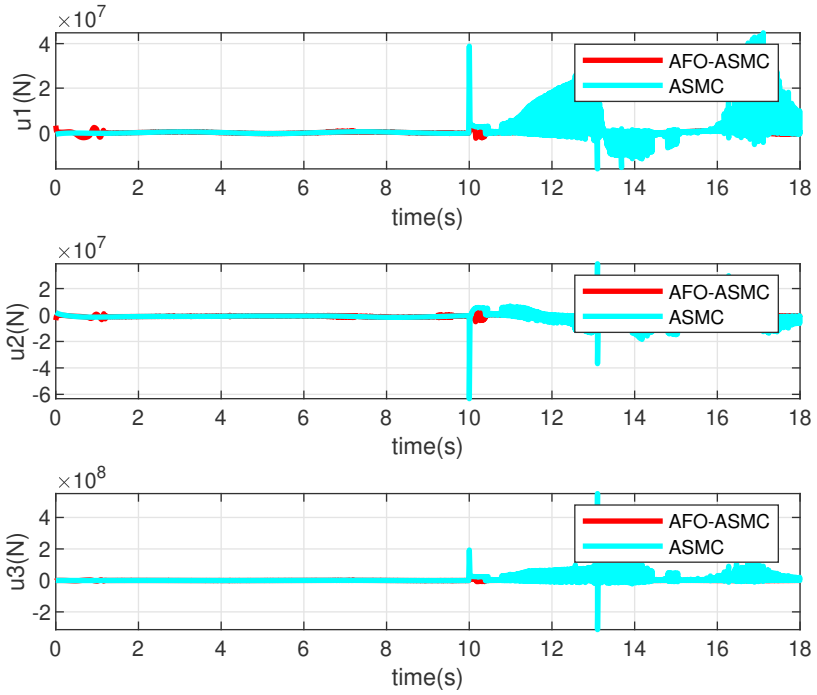

Figure 10: Attitude control signal

Through Fig. 10, it is evident that the control input signal of ASMC is generally larger than that of AFO-ASMC. This indicates that our designed control method effectively reduces system gain, minimizing system input control as much as possible. Additionally, beyond time $t = 10$, we introduced non-matching disturbances. Although the attitude signal of ASMC was not significantly affected, its control input suddenly increased, approaching or exceeding the control limits of the RLV. This is a situation that should be avoided in control applications. In contrast, AFO-SMC did not exhibit such behavior, highlighting the practicality of the proposed method.

6. Conclusion

This article presents a new adaptive multivariable attitude tracking control scheme for RLV with bounded but unknown external interferences and uncertainties. The mismatched interferences were replaced by a new state by designing an AFO, which resulted in a new RLV attitude control system. A non-overestimated adaptive gain was designed to construct the adaptive multivariable attitude control algorithm, which has an important feature of being easy to implement and ensuring that the attitude tracking error converges to pre-specified performance regions without being affected by external interferences. The Lyapunov stability of the proposed method has been proven, and

the theoretical results show that the system's state can always stay in the designated region. Finally, the merits of the proposed control scheme were highlighted by performing simulation case studies.

References

[1] P. P. Menon, I. Postlethwaite, S. Bennani, A. Marcos, D. Bates, Robustness analysis of a reusable launch vehicle flight control law, Control Engineering Practice 17 (7) (2009) 751–765.

[2] Y. Wang, Y. Wang, Z. Jiang, Numerical investigation of aerodynamic separation schemes for two-stage-to-orbit-like two-body system, Aerospace Science and Technology 131 (2022) 107995.

[3] Q. Mao, L. Dou, Q. Zong, Z. Ding, Attitude controller design for reusable launch vehicles during reentry phase via compound adaptive fuzzy h-infinity control, Aerospace Science and Technology 72 (2018) 36–48.

[4] X. Zhang, R. Mu, J. Chen, P. Wu, Hybrid multi-objective control allocation strategy for reusable launch vehicle in re-entry phase, Aerospace Science and Technology 116 (2021) 106825. doi:https://doi.org/10.1016/j.ast.2021.106825.

[5] B. Tian, Z. Li, X. Zhang, Q. Zong, Adaptive prescribed performance attitude control for rlv with mismatched disturbance, Aerospace Science and Technology 117 (2021) 106918. doi:https://doi.org/10.1016/j.ast.2021.106918.

[6] L. Ye, B. Tian, H. Liu, Q. Zong, B. Liang, B. Yuan, Anti-windup robust backstepping control for an underactuated reusable launch vehicle, IEEE Transactions on Systems, Man, and Cybernetics: Systems.

[7] M. Kerr, A. Marcos, L. Peñin, E. Bornschlegl, Gain scheduled fdi for a re-entry vehicle, in: AIAA Guidance, Navigation and Control Conference and Exhibit, 2008, p. 7266.

[8] S. Bharadwaj, A. V. Rao, K. D. Mease, Entry trajectory tracking law via feedback linearization, Journal of Guidance, Control, and Dynamics 21 (5) (1998) 726–732.

[9] J. Reiner, G. J. Balas, W. L. Garrard, Flight control design using robust dynamic inversion and time-scale separation, Automatica 32 (11) (1996) 1493–1504.

[10] J. D. Schierman, D. G. Ward, J. R. Hull, N. Gandhi, M. Oppenheimer, D. B. Doman, Integrated adaptive guidance and control for re-entry vehicles with flight test results, Journal of Guidance, Control, and Dynamics 27 (6) (2004) 975–988.

[11] J. Yu, P. Shi, L. Zhao, Finite-time command filtered backstepping control for a class of nonlinear systems, Automatica 92 (2018) 173–180.

[12] R. Chai, A. Tsourdos, H. Gao, S. Chai, Y. Xia, Attitude tracking control for reentry vehicles using centralised robust model predictive control, Automatica 145 (2022) 110561.

[13] M. Sagliano, E. Mooij, S. Theil, Adaptive disturbance-based high-order sliding-mode control for hypersonic-entry vehicles, Journal of Guidance, Control, and Dynamics 40 (3) (2017) 521–536.

[14] C. Edwards, S. Spurgeon, Sliding mode control: theory and applications, Crc Press, 1998.

[15] Y. Shtessel, L. Fridman, F. Plestan, Adaptive sliding mode control and observation, International Journal of Control 89 (9) (2016) 1743–1746.

[16] Y. Shtessel, C. Hall, M. Jackson, Reusable launch vehicle control in multiple-time-scale sliding modes, Journal of Guidance, Control, and Dynamics 23 (6) (2000) 1013–1020.

[17] S. E. Talole, J. P. Kolhe, S. B. Phadke, Extended-state-observer-based control of flexible-joint system with experimental validation, IEEE Transactions on Industrial Electronics 57 (4) (2009) 1411–1419.

[18] B. Tian, Q. Zong, J. Wang, F. Wang, Quasi-continuous high-order sliding mode controller design for reusable launch vehicles in reentry phase, Aerospace science and technology 28 (1) (2013) 198–207.

[19] B. Tian, L. Yin, H. Wang, Finite-time reentry attitude control based on adaptive multivariable disturbance compensation, IEEE Transactions on Industrial Electronics 62 (9) (2015) 5889–5898.

[20] Z. Guo, J. Chang, J. Guo, J. Zhou, Adaptive twisting sliding mode algorithm for hypersonic reentry vehicle attitude control based on finite-time observer, ISA transactions 77 (2018) 20–29.

[21] Y. Shtessel, M. Taleb, F. Plestan, A novel adaptive-gain supertwisting sliding mode controller: Methodology and application, Automatica 48 (5) (2012) 759–769.

[22] B. Tian, J. Cui, H. Lu, Z. Zuo, Q. Zong, Adaptive finite-time attitude tracking of quadrotors with experiments and comparisons, IEEE Transactions on Industrial Electronics 66 (12) (2019) 9428–9438.

[23] H. Xu, M. D. Mirmirani, P. A. Ioannou, Adaptive sliding mode control design for a hypersonic flight vehicle, Journal of guidance, control, and dynamics 27 (5) (2004) 829–838.

[24] D. Ginoya, P. Shendge, S. Phadke, Sliding mode control for mismatched uncertain systems using an extended disturbance observer, IEEE Transactions on Industrial Electronics 61 (4) (2013) 1983–1992.

[25] X. Yu, P. Li, Y. Zhang, The design of fixed-time observer and finite-time fault-tolerant control for hypersonic gliding vehicles, IEEE Transactions on Industrial Electronics 65 (5) (2017) 4135–4144.

[26] J. Yang, S. Li, C. Sun, L. Guo, Nonlinear-disturbance-observer-based robust flight control for airbreathing hypersonic vehicles, IEEE Transactions on Aerospace and Electronic systems 49 (2) (2013) 1263–1275.

[27] J. Davila, Exact tracking using backstepping control design and high-order sliding modes, IEEE Transactions on Automatic Control 58 (8) (2013) 2077–2081.

[28] A. Chalanga, S. Kamal, L. M. Fridman, B. Bandyopadhyay, J. A. Moreno, Implementation of super-twisting control: Super-twisting and higher order sliding-mode observer-based approaches, IEEE Transactions on Industrial Electronics 63 (6) (2016) 3677–3685.

[29] L. Wu, Y. Gao, J. Liu, H. Li, Event-triggered sliding mode control of stochastic systems via output feedback, Automatica 82 (2017) 79–92.

[30] B. Tian, Z. Li, X. Zhao, Q. Zong, Adaptive multivariable reentry attitude control of rlv with prescribed performance, IEEE Transactions on Systems, Man, and Cybernetics: Systems.

[31] A. F. Filippov, Differential equations with discontinuous righthand sides: control systems, Vol. 18, Springer Science & Business Media, 2013.

[32] S. P. Bhat, D. S. Bernstein, Continuous finite-time stabilization of the translational and rotational double integrators, IEEE Transactions on automatic control 43 (5) (1998) 678–682.

[33] S. Khoo, L. Xie, S. Zhao, Z. Man, Multi-surface sliding control for fast finite-time leader–follower consensus with high order siso uncertain nonlinear agents, International Journal of Robust and Nonlinear Control 24 (16) (2014) 2388–2404.

[34] J. Liu, S. Laghrouche, M. Harmouche, M. Wack, Adaptive-gain second-order sliding mode observer design for switching power converters, Control Engineering Practice 30 (2014) 124–131.

[35] Z. Wang, D. Yang, T. Ma, N. Sun, Stability analysis for nonlinear fractional-order systems based on comparison principle, Nonlinear Dynamics 75 (2014) 387–402.

[36] J. A. Moreno, D. Y. Negrete, V. Torres-González, L. Fridman, Adaptive continuous twisting algorithm, International Journal of Control 89 (9) (2016) 1798–1806.

[37] Y. B. Shtessel, J. A. Moreno, L. M. Fridman, Twisting sliding mode control with adaptation: Lyapunov design, methodology and application, Automatica 75 (2017) 229–235.

[38] R. A. Horn, C. R. Johnson, Matrix analysis, Cambridge university press, 2012.

[39] B. Tian, W. Fan, R. Su, Q. Zong, Real-time trajectory and attitude coordination control for reusable launch vehicle in reentry phase, IEEE Transactions on Industrial Electronics 62 (3) (2014) 1639–1650.

[40] Q. Mao, L. Dou, Z. Yang, B. Tian, Q. Zong, Fuzzy disturbance observer-based adaptive sliding mode control for reusable launch vehicles with aeroservoelastic characteristic, IEEE Transactions on Industrial Informatics 16 (2) (2020) 1214–1223. doi:10.1109/TII.2019.2924731.

[41] C. P. Bechlioulis, G. A. Rovithakis, Adaptive control with guaranteed transient and steady state tracking error bounds for strict feedback systems, Automatica 45 (2) (2009) 532–538.

[42] J. Kochalummoottil, Y. B. Shtessel, J. A. Moreno, L. Fridman, Output feedback adaptive twisting control: A lyapunov design, in: 2012 American Control Conference (ACC), IEEE, 2012, pp. 6172–6177.

[43] H. Obeid, L. M. Fridman, S. Laghrouche, M. Harmouche, Barrier function-based adaptive sliding mode control, Automatica 93 (2018) 540–544.

https://dspace.org/

Adaptive multivariate reusable launch vehicles reentry attitude control with pre-specified performance in the presence of unmatched disturbances

Ge, Tianshuo; Chai, Runqi; Zhu, Qinghua; Chen, Kaiyuan; Tsourdos, Antonios ...

2024-02-01
Elsevier
https://doi.org/10.1016/j.ast.2023.108858
Ge T, Chai R, Zhu Q, et al., (2024) Adaptive multivariate reusable launch vehicles reentry attitude control with pre-specified performance in the presence of unmatched disturbances. Aerospace Science and Technology, Volume 145, February 2024, Article number 108858

Downloaded from a DSpace repository. https://dspace.org/